Comunicações Geológicas

Comunicações Geológicas (2023) 110, 1, 39-60
ISSN: 0873-948X; **e-ISSN:** 1647-581X

The post-breakup magmatism in Cabo Frio High, Campos Basin, Brazil: implications to a thinned lithosphere contribution in magma formation

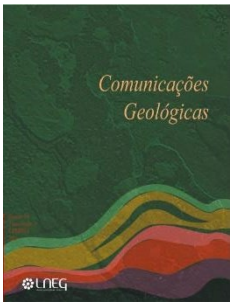

O magmatismo pós-fragmentação no Alto de Cabo Frio, Bacia de Campos, Brasil: implicações para a contribuição de uma litosfera adelgaçada na formação de magma

T. M. J. de Barros[1]*, P. C. Brito[1], A. Corval[1], S. C. Valente[1], A. W. A. Miranda[1]

DOI: https://doi.org/10.34637/h145-3n13
Recebido em 04/04/2023 / Aceite em 10/10/2023
Publicado online em novembro de 2023

Artigo original
Original article

Abstract: The Cabo Frio High, limit between Campos and Santos basins, consists of an elevated structure characterized by intense magmatism. Through new petrographic and geochemical data, this paper brings new highlights on sources and evolutionary processes associated with volcanic events that affected this area during Santonian-Campanian drifting stage. Samples from three studied wells are pyroclastic ash, lapilli tuffs, basalts, scoria and diabases associated with subaerial explosive volcanism. Geochemically, they are alkaline rocks classified as basalts, alkaline basalts, foidites and tephriphonolites. The evolution of these rocks derives from geodynamic processes that occurred in shallow mantle depths (35 – 80 km) and involved mixing between a depleted, relatively shallow asthenospheric source (N-MORB) and the local subcontinental lithospheric mantle represented by the average composition of the lamprophyres at the Cabo Frio Structural High.

Keywords: Volcanism, lithogeochemistry, Cabo Frio High.

Resumo: O Alto de Cabo Frio, limite entre as bacias de Campos e Santos, é uma estrutura elevada caracterizada por intenso magmatismo. Novos dados petrográficos e geoquímicos deste trabalho fornecem novas perspetivas acerca das fontes e processos evolucionários associados a eventos vulcânicos que afetaram esta área durante o Santoniano-Campaniano. Amostras de poços estudados são cinzas piroclásticas, lapilli tufos, basaltos, escórias e diabásios associados com um vulcanismo subaéreo explosivo. Geoquimicamente, são rochas alcalinas classificadas como basaltos, basaltos alcalinos, foiditos e tefrifonolitos. A evolução dessas rochas deriva de processos geodinâmicos que ocorreram a profundidades reduzidas no manto (35 – 80 km) e envolveram a mistura entre uma fonte astenosférica relativamente superficial e esvaziada (N-MORB) e o manto litosférico subcontinental local representado pela composição média dos lamprófiros do Alto Estrutural de Cabo Frio.

Palavras-chave: Vulcanismo, litogeoquímica, Alto de Cabo Frio.

[1] Postgraduate Program in Modeling and Geological Evolution, Federal Rural University of Rio de Janeiro, Seropédica, Rio de Janeiro 23890-000, Brazil.

* Corresponding author / Autor correspondente: tatielemarques@ufrrj.br

1. Introduction

The southeastern Brazilian continental margin basins are important areas of oil and gas exploration. Hydrocarbon systems are intrinsically associated with their tectonic, stratigraphic and magmatic development. Igneous events can provide a thermal increment in source rocks that leads to organic matter maturation. Furthermore, magmatic rocks might be important seals, reservoirs or paths to oil and gas occurrences (Thomaz Filho *et al*., 2008).

The tectonic evolution of sedimentary basins in southeastern Brazil is related to the opening of the South Atlantic Ocean. This event started in the Upper Cretaceous and evolved to the Gondwana breakup. The consequent African and South American continents separation produced all sedimentary basins on the east Brazilian margin, such as Espírito Santos, Campos, and Santos basins (Moreira, 2007).

Magmatic events in such rifted to passive margins are commonly referred to as associated with different tectonic evolutionary processes: lithosphere stretching efforts (*e.g.* Franke, 2013), reactivation of major structures (Almeida, 1983; Oreiro *et al.*, 2008) and plume-related magmatism (Thompson *et al.,* 1998; Thomaz Filho and Rodrigues, 1999; Thomaz Filho *et al.*, 2005). Still, limited petrological studies comprising especially drift stage magmatism in Santos and Campos basins turned difficult to determine possible geotectonic processes and sources involved in such events.

The Cabo Frio High, an elevated structure between these two basins, encompasses important occurrences of the magmatism that affected the sedimentary evolution of Campos and Santos basins (Oreiro, 2006; Moreira, 2007; Winter, 2007; Oreiro *et al.*, 2008). The study of the magmatism that occurred in this area represents a key element to understand how tectonomagmatic processes can influence such marginal basin development and even how they can modify petroliferous systems, so important to the exploration of oil and gas in these basins.

Therefore, this paper aims to contribute with the generation of new data by characterizing petrographically volcanic and volcaniclastic rocks sampled in the Cabo Frio High area (Fig. 1). Additionally, petrogenetic and geodynamic models proposed enlighten different processes and possible sources associated with this mafic magmatism.

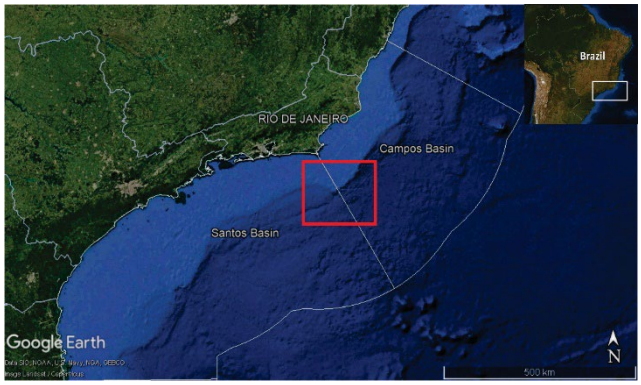

Figure 1. Schematic map showing the Cabo Frio High region and the limit between the Santos and Campos basins. The study area is highlighted by the red rectangle on the map.

Figura 1. Mapa esquemático mostrando a região do Alto de Cabo Frio e o limite entre as bacias de Santos e Campos. A área de estudo é destacada pelo retângulo vermelho no mapa.

2. Geological Setting

The Santos and Campos basins are located in the southeastern Brazilin margin. Their tectonic evolution is associated with rifting and lithospheric stretching processes that led to a Late Aptian break-up between the South America and Africa lithosphere. As a result of these extensional events, normal faults systems and accommodation zones (horsts and grabens) were created in the Pre-Cambrian basement and controlled uppermost posterior sedimentation. Subsequent opening of the South Atlantic Ocean and continuous extensional efforts led to an evolution from rift to passive continental margin basin (Chang *et. al*., 1992, Cainelli and Mohriak, 1999).

Santos and Campos crystalline basement consists of the Cabo Frio and Oriental terrains from the Neoproterozoic Ribeira Orogen. These terrains related to the Braziliano orogenic collage, are characterized by compressional, metamorphic and magmatic episodes. This orogeny generated metasedimentary and metavolcano-sedimentary association, besides pre-to-pos collisional granitoid (e.g., Heilbron *et al*., 2000; Schmitt *et al*., 2004; Tupinamba *et al*., 2007; Schmitt *et al*., 2008).

These basins stratigraphic and sedimentary evolution comprises three main phases: rift, post-rift and drift supersequences (Moreira *et al*., 2007; Winter *et al*., 2007), also denominated continental, transitional evaporitic/shallow carbonate and open-marine, or continental, transitional and marine megasequences, respectively (Chang *et. al*, 1992, Cainelli and Mohriak, 1999).

Both basins were affected by important magmatic events during their evolution. The first event recorded consists of the pre-to-synrift-related floods of the Cabiúnas (Campos Basin) and Camboriú (Santos Basin) formations (Moreira *et al*., 2007; Winter *et al*., 2007). Dating from 137 to 122 (Ar-Ar), these rocks are mainly subereous and subaqueous tholeiitic basalt, occasionally diabase and volcaniclastics rocks (Mohriak *et al.*, 2021; Mizusaki *et al.*, 1988; De Luca *et al.*, 2015).

The two subsequent magmatic events are characterized by basaltic floods and intrusions that occur during the syn-to-post rift phase and are associated with salt and pre-salt layers. These rocks are classified as basalts and originate from magmas with sub-alkaline tholeiitic to transitional composition (Moreira *et al*., 2007; Winter *et al.*, 2007; Mohriak *et al.*, 2021). Low TiO_2 and high MgO_2 content in these basalts indicate a possible interaction between volcanism and water, as well assimilation of contaminants from the local lower crust (Lobo, 2007; Dani *et al*., 2017). The limited studies and geochronological data might suggest that these two magmatic occurrences are possibly related and part of one major event (Gordon *et al.*, 2013).

The drift phase in Campos and Santos basins exhibits two main magmatic pulses between the Santonian-Campanian (around 85 - 75 Ma) and the Lower Eocene (around 50 Ma). Both are characterized by intrusive and extrusive alkaline rocks including basalts, diabases trachyte, syenite, phonolite, nepheline syenite. Volcaniclastic material is also present, as well as the ones observed in the "3-Fingers" and the "3B" marks in Campos Basins (Almeida *et al*., 1996; Alves, 2006; De Luca *et al.*, 2015).

Although adjacent to the Campos and Santos Basins, the Cabo Frio High shows significant differences in its structural and stratigraphic styles from the surrounding area (Mohriak *et al*., 1995). It comprises an elevated structure of the basement that separates the Campos and Santos basin. This high extends across the continental shelf and by the São Paulo Plateau serving as a barrier to sedimentation between the two basins (Pedro, 2005).

Another difference between the Cabo Frio High and the adjacent regions is its large volume of magmatism. The magmatic rocks are both extrusive and intrusive in different stratigraphic levels. They occur as floods, sills, dikes, and mostly as volcanic cones identified in seismic sections (Fig. 2) (Mizusaki and Mohriak, 1992; Oreiro, 2006; Moreira *et al.*, 2005, Rangel, 2006). Associated with this volcanism there is a record of a thick volcanoclastic sequence that sometimes has a slope that plunges towards the continent (Oreiro, 2006). The rocks aforementioned occur in water depths greater than 500 meters (Misuzaki and Mohriak, 1992; Mohriak *et al.*, 2003).

As well as observed in other regions of Campos and Santos Basin, the Cabo Frio High magmatism was observed from the Late Cretaceous to the Eocene (Fig. 3). A subdivision specifically proposed for this region is based on seismic, petrographic, chemical, and radiometric data (Mohriak *et. al*., 1990; Mizusaki and Mohriak, 1992):

I. Sequence I – Composed by the basalts of Cabiúnas Formation (120-130 Ma, Eocretacic). These rocks are correlated to the Camboriú Formation at Santos Basin and Serra Geral Formation at Parana Basin.
II. Sequence II – Composed predominantly of basalts with little representation and Campanian-Turonian age (80 – 90 Ma).
III. Sequence III – Basalts, diabases, and volcanoclastic rocks with ages from Early Paleocene to Eocene (40 – 50 Ma).

Some authors point out that the most significant magmatic event around the Cabo Frio region began in the Albian (Oreiro and Guerra, 2005), reached its climax in the Eocene (Mizusaki and Mohriak, 1992), and is associated with great uplift of the continental crust, which is correlated to an NW-SE lineament that is extending from the oceanic crust (around the region of Jean Charcot mounts) until the Cabo Frio High (Zalan and Oliveira, 2005).

Ultimately, the magmatic events in Campos and Santos basins are time-correlated based on the most recent proposals for their chronostratigraphic columns, even though the drift-related, Cretaceous-Paleogene magmatism has been recorded only in Santos (Fig. 4).

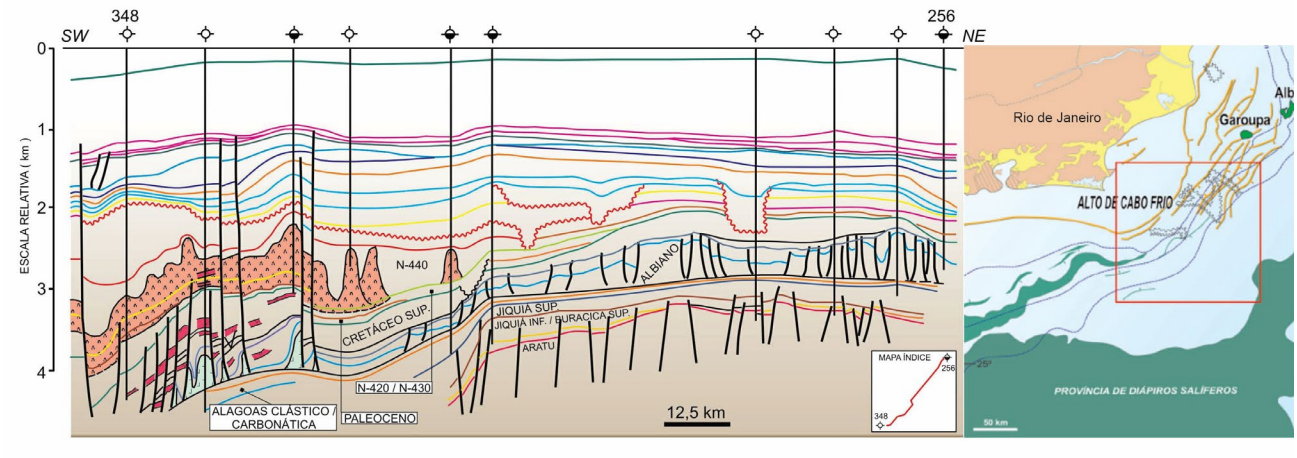

Figure 2. South Campos Basin geological section. Volcanic cones are evidenced by seismic lines (Modified from Rangel, 2006).

Figura 2. Seção geológica do sul da Bacia de Campos. Cones vulcânicos são evidenciados por linhas sísmicas (Modificado de Rangel, 2006).

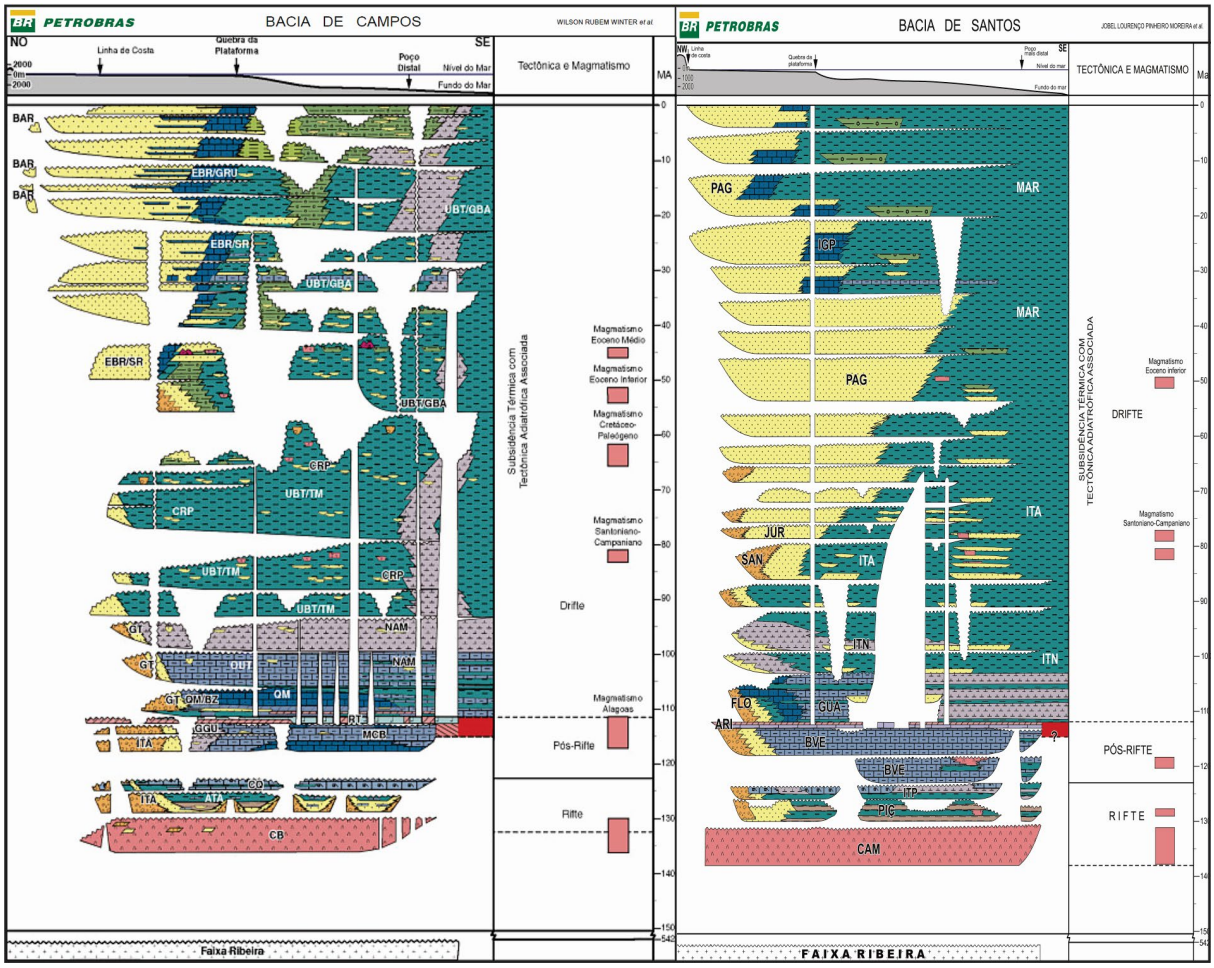

Figure 3. Campos and Santos basins chronostratigraphic chats. Magmatic events are indicated in red rectangles (Modified from Moreira *et al*., 2007; Winter *et al*., 2007).

Figura 3: Cartas Cronoestratigráficas das bacias de Campos e Santos. Eventos magmáticos estão indicados nos retângulos vermelhos (Modificado de Moreira *et al*., 2007; Winter *et al*., 2007).

Alkaline basalt flows and intrusions with 83.2 to 72.4 Ma, as well ash hyaloclastites and bentonites (the so-called 3-Fingers Mark; Marco 3-Dedos), occur mainly in the south area of Campos Basin and represent the drift-related, Santonian-Campanian magmatism (Mizusaki *et al*., 1992; Winter *et al*., 2007). The 1m-thick, widespread bentonites (Marco 3-Dedos) are taken as altered, volcanic

ash deposits interbedded with the marine sediments of the Ubatuba Formation that were originated from a Plinian explosive volcanism (Caddah *et al.*, 1994; Alves, 2006). On the other hand, the so-called 3B Mark (Marco 3B) is thought to represent reworked pyroclastic ash that falls from the same emission centers that formed the bentonites. These volcanoclastic sediments mixed with siliciclastic accumulated on the continental shelf where they were further reworked to give rise to Maastrichtian turbidites (Alves, 2006).

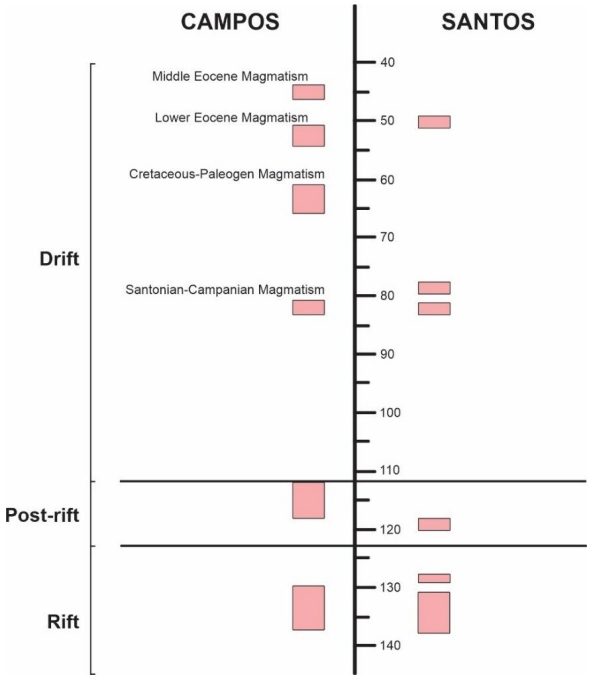

Figure 4. Time correlation of the magmatic processes recorded in Santos and Campos basins (Modified from Moreira *et al.*, 2007; Winter *et al.*, 2007).

Figura 4. Correlação temporal dos processos magmáticos registrados nas bacias de Campos e Santos (Modificado de Moreira *et al.*, 2007; Winter *et al.*, 2007).

As referred before, the studied area is located nearby the Cabo Frio Structural High between Santos and Campos basins. Well profiles indicate that the selected magmatic sections are observed in association with shales and marls of the Tamoios Member (Ubatuba Formation) and underlying sandstones of the Carapebus Formation, likely to be linked to the Santonian-Campanian drift magmatism in the Campos Basin. The time-correlated magmatism in the adjoining continental area is recorded in the northern sector of the Serra do Mar Alkaline Province and the Poços de Caldas-Cabo Frio Magmatic Alignment and has been associated with either interaction between lithospheric and asthenospheric Trindade plume-like mantle sources or reactivation of deep-seated lithospheric faults (Thomaz Filho and Rodrigues, 1999; Thomaz Filho and Misuzaki, 2008; Almeida, 1983; Riccomini *et al.*, 2005).

3. Materials and methods

Materials used in this study consist of well profiles, sidewall and drill cutting samples organized in magmatic sections of three wells. Well profiles were described and samples from post-salt magmatic sections were selected for petrographic and lithogeochemical analysis. When extracted from oil wells, rock samples are exposed to drilling mud which can leave residues that might affect the rock's chemical composition when not removed. Samples were then washed in running water with the assistance of a soft brush for better removal of impurities.

Once dry, drill cutting samples were sieved for loss of fines with two-particle size screens, #48 and #100 respectively. The material retained in the # 100 sieve was stored in 4x4 cm ziplock bags, with the corresponding depth interval for each sample.

The material retained in the # 48 sieve was divided into two rates: magnetic and non-magnetic samples. Both aliquots were grouped by textural type according to color and texture (such as "phaneritic gray" and "aphanitic black") (Fig. 5). This separation was performed to classify different magmatic lithologies and their estimated depth in the studied sections. Each sample group was stored in a 4x4 cm ziplock bag identified with corresponding code and depth interval.

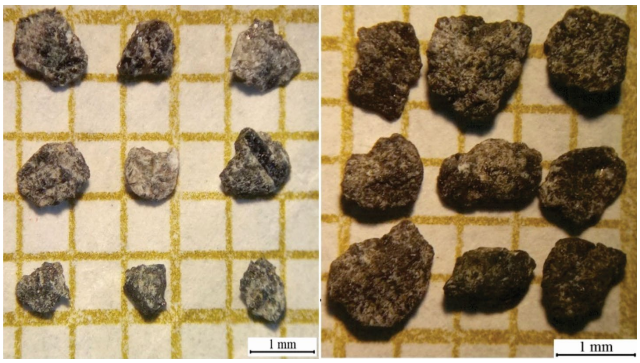

Figure 5. Macroscopic view of drill cutting samples. Separation process evolved the identification of different textural groups divided according to characteristics such as magnetism and color.

Figura 5. Visão macroscópica de amostras de calhas. Processo de separação envolveu a identificação de diferentes grupos texturais divididos de acordo com características como magnetismo e cor.

Sidewall and selected drill cutting samples were laminated and microscopic descriptions were made using a transmitted-light petrographic microscope Zeiss Axio. Thin section pictures were obtained using a Zeiss Microscope Axio Imager A2 petrographic. These analyses were performed at the Federal Rural University of Rio de Janeiro – Department of Petrology and Geotectonics laboratory.

Lithogeochemical data for fifteen sidewall samples were obtained at the ACTLABS in Canada. Major elements (SiO_2, TiO_2, Al_2O_3, $Fe_2O_3^t$, MnO, MgO, CaO, Na_2O, K_2O, P_2O_5) concentrations (in wt.%) were obtained by Inductively Coupled Plasma-Atomic Emission Spectrometry (ICP-AES) whereas selected trace elements (Ba, Rb, Sr, Zr, Y, Nb, Ni, Cr, V, Co, U, Th, Hf, Ta and Pb), including the whole set of rare earth elements (La, Ce, Pr, Nd, Sm, Eu, Gd, Tb, Dy, Ho, Er, Tm, Yb e Lu), were measured (in ppm) by Inductively Coupled Plasma-Mass Spectrometry (ICP-MS). The loss of ignition (LOI) was measured by weight differences between ignited and non-ignited samples. Iron was measured as total iron as ferric iron (Fe_2O_{3t}). Analytical precision for major elements measured based on duplicates was between 0.3% and 1.7%, whereas for the selected trace elements was between 0.3% and 2.7% and between 0.5% and 7.9% for the rare earth elements (REE). Analytical accuracy for major elements was calculated based on element concentrations of international standards and was between 0.6% and 6.9%. For trace elements, the accuracy was between 1.0% and 3.39% and between 1.5% and 12.5% for the REE.

4. Results

4.1. Well Data

Schematic sections of wells EG1, EG2 and EG3 are shown in figure 6. Rocks shown in the three sections are stratigraphically above the salt sequence.

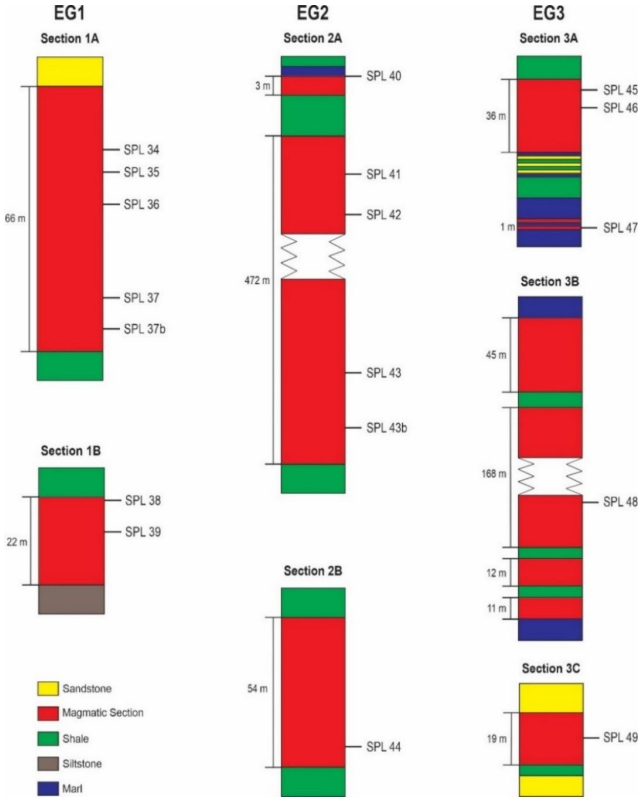

Figure 6. Schematic sections of wells EG1, EG2 and EG3 in northern Santos Basin. Sidewall core samples (SPL) are indicated.

Figura 6. Seções esquemáticas dos poços EG1, EG2 e EG3 no norte da Bacia de Santos. Amostras laterais (SPL) são indicadas.

Two magmatic sections were studied in well EG1. Section 1A is a 66 m thick continuous occurrence of dark gray magmatic rocks. These rocks underlie sandstones (Carapebus Formation) and overlie shales (Ubatuba Formation). Section 1B is a 22 m thick continuous occurrence of a diabase associated to shales and marls of the Ubatuba Formation (Tamoios Member). Both sections in well EG2 (2A; 483.5 m thick and 2B; 54 m thick) consist of lapilli tuffs that occur overlain and underlain by shales of the Ubatuba Formation. The well EG3 comprises three magmatic sections, as such: Section 3A comprises 35 m thick and 1 m thick occurrences of magmatic rocks interlayered with shales, sandstones, and marl of the Ubatuba Formation. Section 3B is a 236 m thick occurrence of magmatic rocks interlayered with three thin shale beds. Section 3C is a 19 m thick occurrence of magmatic rocks overlain and underlain by sandstones and shales of the Ubatuba Formation.

4.2. Petrography

4.2.1. Sidewall Core Samples

Well EG1

Pyroclastic lithic ash tuffs with lithoclasts of trachyte (both aphyric and porphytiric) occur in section 1A (Fig. 7A), as well as olivine-phyric agglutinated scoria (Fig. 7B), and crystalloclasts of pyroxene and alkali feldspar (Fig. 7C). The flat shape of vesicles in scoria indicates the presence of spatter cones. The occurrence of trachyte lithoclasts indicates and alkaline basalt-trachyte rock association typical of mildly alkaline series. This magmatic section's intermediate and uppermost rocks are also represented by centimetric bedding that alternates glass-, lithoclast- and carbonate-cemented, and crystalloclast-rich beds. Crystalloclasts are plagioclase, nepheline, biotite and opaque minerals. Clasts of glass are also observed. Some samples may represent mixed volcanoclastic tuffaceous sandstones with little reworking as depicted by the angular shapes of quartz crystalloclasts. As such, deposition was close to the emission center. There are no textures that can be undoubtedly associated with subaqueous volcanism.

Rocks in Section 1B were classified as alkali diabases (Fig. 7D and E) based on petrographic characteristics. It is difficult to ascertain whether the rocks represent hypabyssal intrusions or flows. However, there are no textures that can be undoubtedly associated with subaqueous volcanism. The top of this magmatic section presents a fine-grained equigranular alkali diabase sample composed of alkali feldspar, clinopyroxene (augite), plagioclase, nepheline (altered to cancrinite), analcime, nosean and devitrified glass (altered to carbonate and chlorite). The partly altered diabase sample is located at the section's intermediate part and is composed of medium-grained plagioclase, alkaline pyroxene and amphibole, biotite, opaque minerals, zircon, apatite, sodalite and devitrified glass (altered to chlorite). Rocks in this section lack textural and structural evidence for pyroclastic processes. The fine- to medium-grained textures might indicate either subvolcanic or volcanic (subaerial), effusive processes.

Well EG2

Five sidewall core samples were used to study the upper, intermediate, and lower parts of section 2A. These rocks present a brecciated texture cemented by carbonate. Lithoclasts are predominantly pyroxene-phyric basalt (Fig. 7F), basaltic scoria (Fig. 7G), and fewer felsic, ash tuffs. The brecciated structure could have resulted from either phreatomagmatism associated with monogenetic scoria cones or hydraulic brecciation caused by coeval hydrothermal vents. The primary or secondary origin of the carbonate cement is difficult to discuss based on petrographic features. Nevertheless, the carbonate is itself fragmented, indicating that the brecciation continued after cementation.

Rocks in magmatic section 2B are lithic lapilli tuffs with lithoclasts of basaltic scoria and alkaline basalts. Lithoclasts are mainly altered, amygdaloidal, aphyric basalt with devitrified-brownish-altered glass (Fig. 7H). Amygdales are irregular in shape and filled with carbonate (Fig. 7I). Magmatism in section 2B comprises an effusive, subaerial basaltic flow at its lower parts whose volcanic environment is similar to the one observed in section 2A.

Well EG3

Three sidewall core samples, that represent the upper and lower parts of section 3A, are altered agglutinated basaltic scoria (Fig. 7J) and ash tuffs. Section 3B comprises one lapilli tuff sample (SPL 48) (Fig. 7K). Fragments includes shards, fiammes, scoria and altered glass. Alteration consists predominantly of chlorite. Compaction is a well-developed structure for very thin deposits (Section 3A) but greater for thicker deposits (Section 3B). Petrographic data obtained for one sidewall core sample (SPL 49) in Section 3C classifies this rock as a welded lapilli tuff with abundant lithoclasts of basaltic scoria (Fig. 7L). Amygdales are predominantly round to sub round, filled with chlorite and carbonate.

4.2.2. Drill Cutting Samples

Drill cutting samples represent a 3-meters interval each with 6 meters depth between them. Due to these technical specificities, the spatial positioning of these magmatic rocks is not as exact as sidewall samples are.

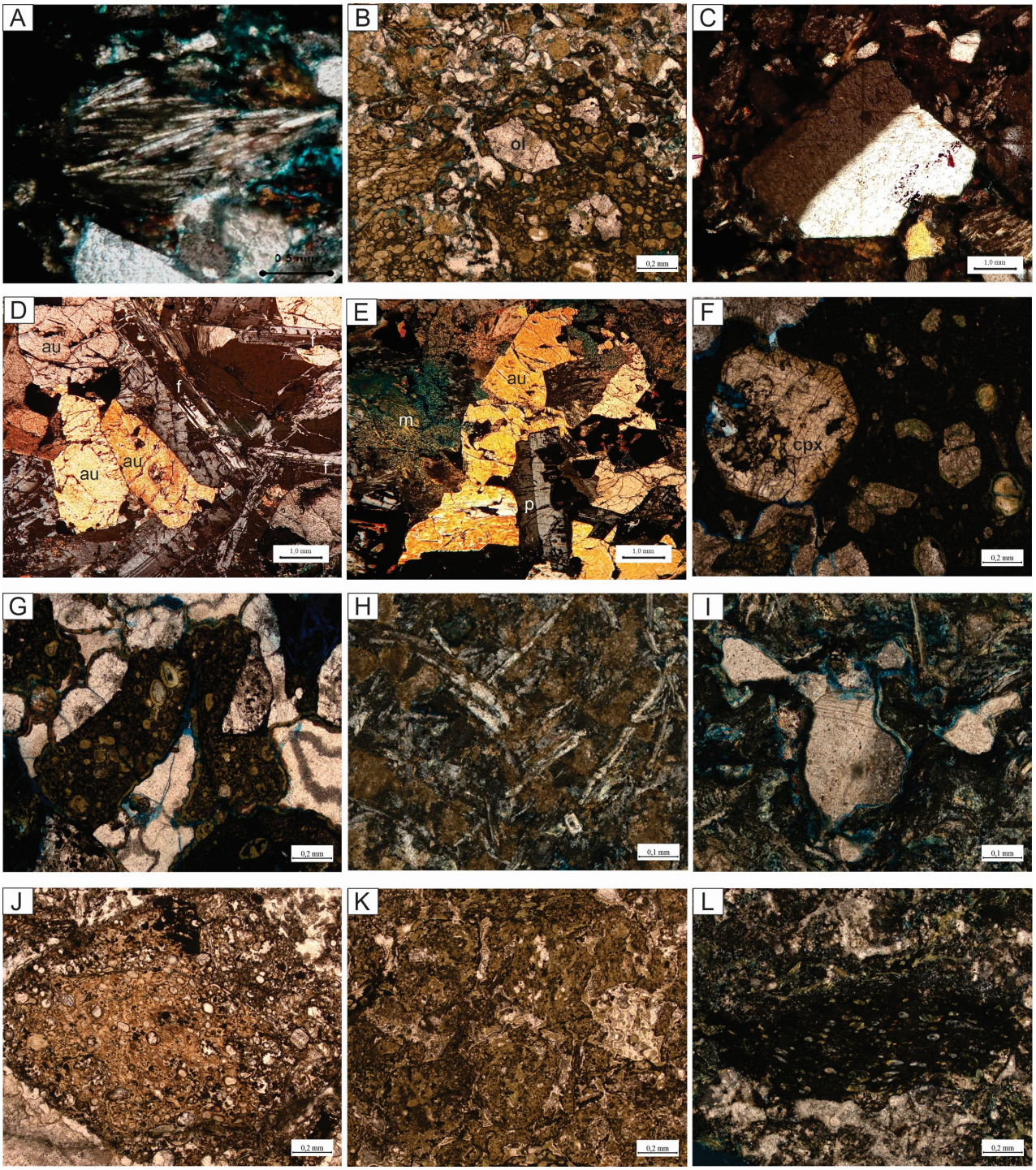

Figure 7. Photomicrographs of sidewall samples from wells EG1, EG2 and EG3. A) lithoclast of trachyte in sample SPL 35 (cross-polarized light); B) lithoclast of scoria with altered olivine (ol) in sample SPL 36 (plane-polarized light); C) alkali feldspar crystalloclast in tuff sample (cross-polarized light); D) equigranular texture in diabase SPL 38 with feldspars (f) and augite (au) (cross-polarized light); E) alkali diabase sample SPL 39 with devitrified glass altered to a mixture of carbonate and chlorite (m), plagioclase (p) and augite (au) (cross-polarized light); F) pyroxene-phyric basalt lithoclast in SPL 41 (cpx = clinopyroxene) (plane-polarized light); G) basaltic scoria lithoclast in SPL 43 (plane-polarized light); H) Aphyric basalt with altered pyroxene and interstitial glass (brown), and plagioclase laths in sample SPL 44 (cross-polarized light); I) irregular carbonate-infilled amygdales in sample SPL 44 (cross-polarized light); J) basaltic scoria lithoclast in SPL 45 (plane-polarized light); K) welded lapilli tuff SPL 48 (plane-polarized light); L) lithoclast of scoria in lapilli tuff SPL 49 (cross-polarized light).

Figura 7. Fotomicrografias de amostras laterais dos poços EG1, EG2 e EG3. A) litoclasto de traquito na amostra SPL 35 (luz polarizada com nicóis descruzados); B) litoclastos de escórias com olivina (ol) na amostra SPL 36 (luz polarizada com nicóis descruzados); C) litoclasto de feldspato alcalino em amostra de tufo (luz polarizada com nicóis cruzados); D) textura equigranular em diabásio SPL 38 com feldspato (f) e augita (au) (luz polarizada com nicóis cruzados); E) amostra de diabásio alcalino SPL 39 com vidro desvitrificado alterado para uma mistura de carbonato e clorita (m), plagioclásio (p) e augita (au) (luz polarizada com nicóis cruzados); F) litoclasto de basalto com pórfiros de piroxênio na SPL 41 (cpx = clinopiroxênio) (luz polarizada com nicóis descruzados); G) litoclasto de escórias basálticas na SPL 43 (luz polarizada com nicóis descruzados); H) basalto afírico com piroxênio alterado e vidro intersticial (marrom) e ripas de plagioclásio na amostra SPL 44 (luz polarizada com nicóis cruzados); I) amígdalas irregulares preenchidas com carbonato na amostra SPL 44 (luz polarizada com nicóis cruzados); J) litoclasto de escória basáltica na SPL 45 (luz polarizada com nicóis descruzados); K) lapilli tufo soldado SPL 48 (luz polarizada com nicóis descruzados); L) litoclasto de escória no lapilli tufo SPL 49 (luz polarizada com nicóis cruzados).

Cutting samples macroscopic and microscopic analyses allowed the identification of different lithologies that were occasionally observed in the same sampled intervals. Additionally, it was possible to estimate their stratigraphic positioning in well profiles (Fig. 8), corroborating and expanding petrographic results obtained with sidewall samples.

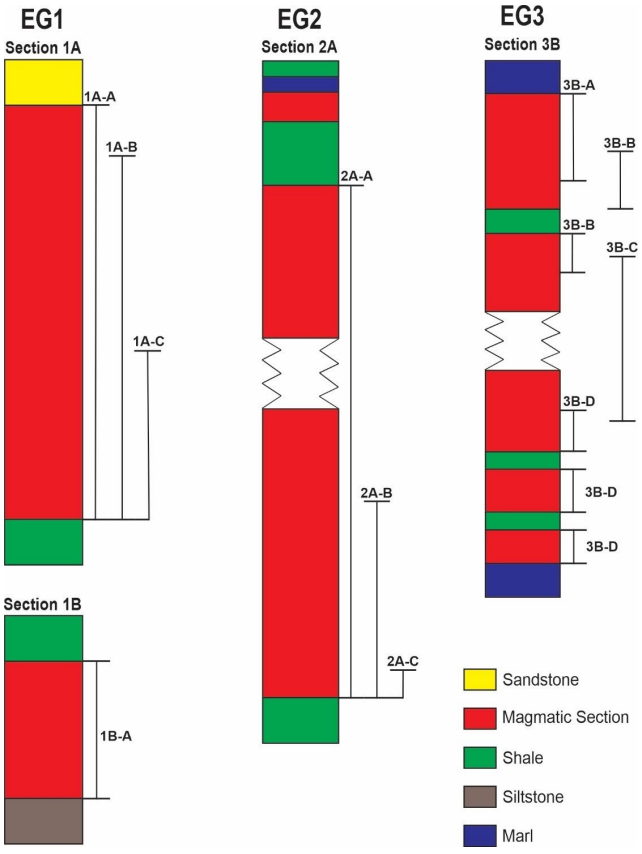

Figure 8. EG1, EG2 and EG3 schematic well profiles, and drill cutting samples magmatic rocks occurrences.

Figura 8. Perfis esquemáticos dos poços EG1, EG2 e EG3, e ocorrências de rochas magmáticas nas amostras de calha.

Well EG1

The uppermost and intermediate portions of Section 1A are, as also observed in sidewall samples, mostly tuffaceous sandstones 1A-A samples (Fig. 9A). These rocks exhibit trachyte lithoclasts, and quartz, biotite, plagioclase and opaque crystalloclasts associated with a micritic matrix. Clasts of altered glass are also present in these samples, as well as rare basalt lithoclasts. Fine-sized lithoclasts and crystalloclasts vary from angular to subangular shape.

Less welded lapilli tuffs (Fig. 9B) are observed predominantly in the intermediate and lowermost parts of Section 1A. These rocks exhibit the same lithoclasts and crystalloclasts observed in 1A-A. Nevertheless, their igneous components are more abundant than sediments, especially the basalt lithoclasts. Lapilli tuffs rich in basaltic scoria lithoclasts are observed mainly in sections deeper portions. Zeolite and carbonate-filled amygdales are very common and vary from spherical to flat shapes. Olivine fine-grained phenocrysts are replaced by carbonate (Fig. 9C).

Section 1B consists of a partially altered diabase intrusion. This rock exhibits clinopyroxene phenocrysts and a coarse-to-medium-grained matrix composed of plagioclase, alkali-feldspar, clinopyroxene (augite), analcime, opaque minerals and apatite (Fig. 9D). Due to size of drill cutting samples, the precise granulometry and intrusive origin of these rocks is difficult to ascertain.

Well EG2

Section 2A is a thick sequence of lapilli tuffs with carbonatic matrix. Lithoclasts consists of porphyritic basaltic scoria (Fig. 9E) and amygdaloidal basalt (Fig. 9F). Sample 2A-A basaltic scoria lithoclasts exhibit altered pseudomorphs phenocrysts and, less frequently, more preserved clinopyroxene medium-grained megacrysts. Amygdales are common and predominantly flat, filled with chlorite, carbonate and zeolite. Amygdaloidal basalt lithoclasts exhibits a glassy matrix with very fine-grained pyroxene and carbonate-filled round amygdales.

Pyroxene-phyric basalt 2A-B exhibits an altered matrix with volcanic glass and fine-grained pyroxene, plagioclase and opaque minerals. Pyroxene phenocrysts are mostly altered with very few preserved grains. Amygdales are irregular and filled with carbonate or zeolite (Fig. 9G).

Sample 2A-C consists of scoria lithoclasts observed predominantly on the bottom portion of Section 2A. Amygdales are variable in size but mostly round and filled with carbonate (Fig. 9H). No mineral was observed among the glassy altered matrix.

Well EG3

Section 3B consists of four volcanic sequences with lapilli tuff, as depicted by the sidewall sample, and basalts, as depicted by drill cutting samples. The top of the section exhibits fine-grained equigranular basalts (Fig. 9I). These rocks are composed essentially of plagioclase, pyroxene, opaque minerals, apatite and volcanic glass. Few zeolite-filled irregular amygdales are present.

Clinopyroxene-phyric basalt 3B-B (Fig. 9J) was also observed associated with the first volcanic sequences. They are characterized by coarse-to-medium-grained phenocrysts, and a fine-grained matrix with pyroxene, plagioclase, opaque minerals, apatite and volcanic glass. Alteration is commonly associated with pyroxene grains. Chlorite-filled amygdales are very rare, but always irregular and flat.

Samples 3B-C are recognized as basalts with coarse-grained phenocrysts. Alteration is common in clinopyroxene megacrysts (Fig. 9K) and in the fine-to-glassy matrix. These rocks occur in the intermediate part of Section 3B.

Another clinopyroxene-phyric basalt occurrence (Fig. 9L) is described in deeper volcanic sequences of Section 3B. These rocks exhibit a fine-grained matrix composed of clinopyroxene, olivine, plagioclase, opaque minerals and volcanic glass. Alteration is commonly observed associated with glassy portions, pyroxene and olivine grains.

4.3. Lithogeochemistry

Studied rocks were geochemically classified based on total alkali *versus* silica (TAS) classification diagram (Fig. 10). Well EG1 rocks (green color) are classified as trachyte, trachy-andesite, basalt trachy-andesite and basanite-tephrite while EG2 samples (blue color) are classified as basanite-tephrite, basalt and foidite. According to the diagram, well EG3 rocks (red color) are classified as basaltic trachy-andesite, basanite tephrite and basalt.

In Harker diagrams, SiO_2, Al_2O_3, Na_2O+K_2O, Y, Sm versus MgO (Figs. 11A, B, D, G and H) and Ti/Y versus Nb/Y

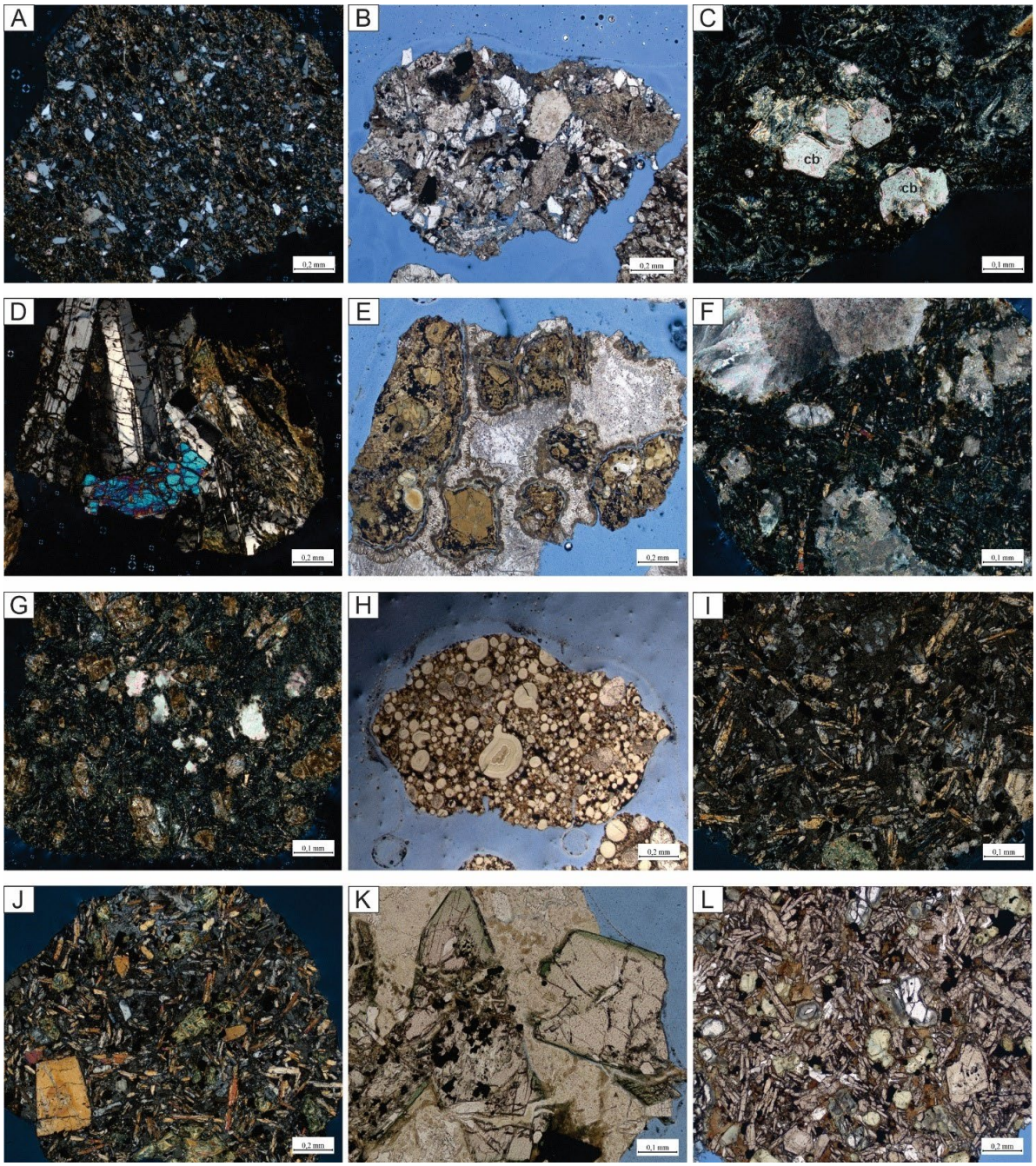

Figure 9. Photomicrographs of drill cutting samples from EG1, EG2 and EG3 wells. A) tuffaceous sandstone 1A-A with angular to subangular crystalloclasts (cross-polarized light); B) medium-welded lapilli tuff 1A-B (plane-polarized light); C) pseudomorphs megacrysts in basaltic scoria lithoclast (1A-C). Original mineral was replaced by carbonate (cb) (cross-polarized light); D) altered diabase intrusion in 1B-A sample (cross-polarized light); E) basaltic scoria lithoclasts in 2A-A lapilli tuff (plane-polarized light); F) amygdaloidal basalt lithoclast in 2A-A lapilli tuff (cross-polarized light); G) porphyritic basalt with carbonate-filled amygdales (2A-B) (cross-polarized light); H) 2A-C scoria sample with carbonate-filled amygdales (plane-polarized light); I) Equigranular basalt 3B-A (cross-polarized light); J) clinopyroxene-phyric basalt in 3B-B sample (cross-polarized light); K) 3B-C sample with partially altered pyroxene phenocryst (plane-polarized light); L) fine-grained matrix in 3B-D sample (plane-polarized light).

Figura 9. Fotomicrografias de amostras de calha dos poços EG1, EG2 e EG3. A) arenito tufáceo 1A-A com cristaloclastos angulares a subangulares (luz polarizada com nicóis cruzados); B) lapilli tufo 1A-B medianamente soldado (luz polarizada com nicóis descruzados); C) megacristais pseudomorfos em litoclasto de escória basáltica (1A-C). O mineral original foi substituído por carbonato (cb) (luz polarizada com nicóis cruzados); D) intrusão de diabásio alterado na amostra 1B-A (luz polarizada com nicóis cruzados); E) litoclastos de escórias basálticas em lapilli tufo 2A-A (luz polarizada com nicóis descruzados); F) litoclasto de basalto amigdaloide em tufo de lapilli 2A-A (luz polarizada com nicóis cruzados); G) basalto porfirítico com amígdalas preenchidas por carbonato (2A-B) (luz polarizada com nicóis cruzados); H) amostra de escória 2A-C com amígdalas preenchidas por carbonato (luz polarizada com nicóis descruzados); I) basalto equigranular 3B-A (luz polarizada com nicóis cruzados); J) basalto com pórfiros de clinopiroxênio na amostra 3B-B (luz polarizada com nicóis cruzados); K) amostra 3B-C com fenocristal de piroxênio parcialmente alterado (luz polarizada com nicóis descruzados); L) matriz de granulação fina na amostra 3B-D (luz polarizada com nicóis descruzados).

(Fig. 12A) present negative pattern while CaO, Cr, Ni *versus* MgO (Figs. 11C, E and F) and Nb/Y *versus* Zr/Y (Fig. 12A) exhibit positive correlation. The square values for the Pearson correlation coefficients (Schober *et al.,* 2018) were calculated for both linear $(R^2)_L$ and polynomial $(R^2)_P$, as well as their respective significance levels (SL_L and SL_P) for a total of n = 15 samples, with

the degree of freedom set as n – 1. Polynomial and linear functions are indicated in diagrams, as well as their respective significance level. As evidenced in both figures 11 and 12, the absence of compositional hiatus suggests that hybridization or simple assimilation processes did not play a significant role in the evolution of these magmas. The distribution and trends observed in Harker diagrams indicate that possible processes of fractional crystallization or AFC (Assimilation and Fractional Crystallization) might have occurred associated to the studied magmatism. The gaps observed in figure 11 are related to reduced sampling. Generally, only in diagrams related to Ni, Y and Sm (Figs. 11C, F, G and H) it is possible to observe subtly better results in polynomial functions when compared to the linear functions. Nevertheless, it is important to highlight that this situation described above could impact the reliability of interpretation and complex petrogenetic discussions in presented Harker diagrams. Figure 12A indicates a negative correlation, suggesting the presence of contamination processes. Nevertheless, the interpretation of this diagram is complicated due to the plot dispersion associated to the low level of significance, probably caused by the problem of sampling hiatus. Conversely, the diagrams presented in figure 12B shows a positive correlation and suggests the absence of contamination processes in the evolution of the studied magmatism.

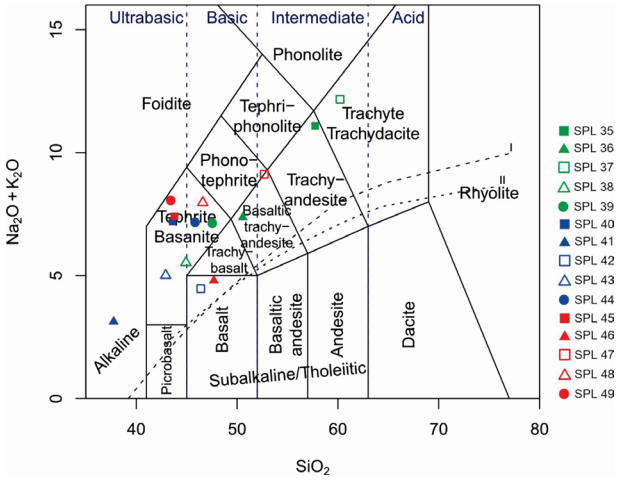

Figure 10. Samples of wells EG1, EG2 and EG3 plotted in the total alkalis *versus* silica (TAS) classification diagram (Le Bas *et al.*, 1986). The subalkaline-alkaline divide curve (dashed line) I is from Irvine and Baragar (1971) and II is from Miyashiro (1978). EG1 represented by green symbols, EG2 represented by blue symbols, EG3 represented by red symbols. Values recalculated to 100% on a volatile-free basis.

Figura 10. Amostras dos poços EG1, EG2 e EG3 representadas no diagrama de classificação de álcalis totais *versus* sílica (TAS) (Le Bas *et al.*, 1986). A curva de divisão subalcalina-alcalina (linha tracejada) I é de Irvine e Baragar (1971) e II é de Miyashiro (1978). EG1 representado por símbolos verdes, EG2 representado por símbolos azuis, EG3 representado por símbolos vermelhos. Valores recalculados para 100% em uma base livre de voláteis.

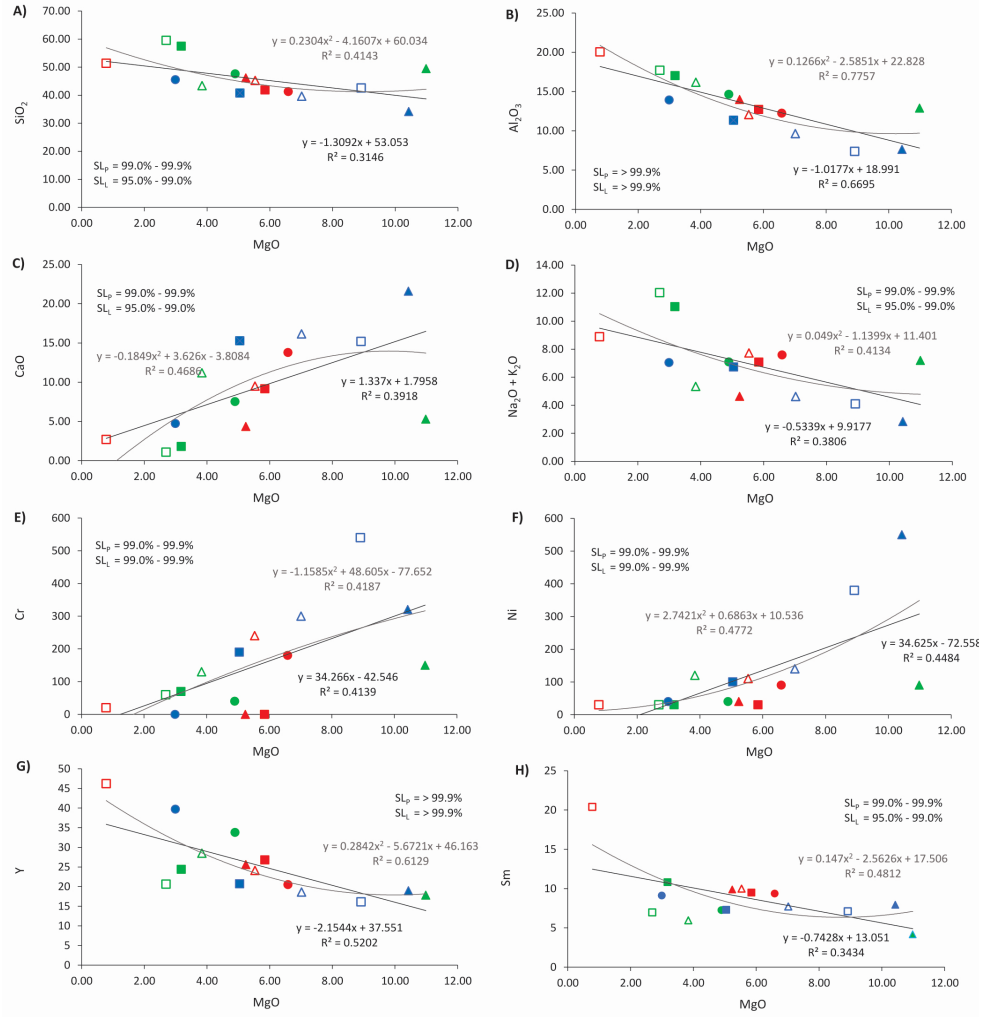

Figure 11. Harker diagrams of major and trace elements for EG1, EG2 and EG3 wells rocks. Samples symbols are same as indicated in figure 11. SL_P = polynomial significance level; SL_L = linear significance level.

Figura 11. Diagramas de Harker de elementos maiores e traço para rochas dos poços EG1, EG2 e EG3. Símbolos das amostras são os mesmos que os indicados na figura 11. SL_P = nível de significância polinomial; SL_L = nível de significância linear.

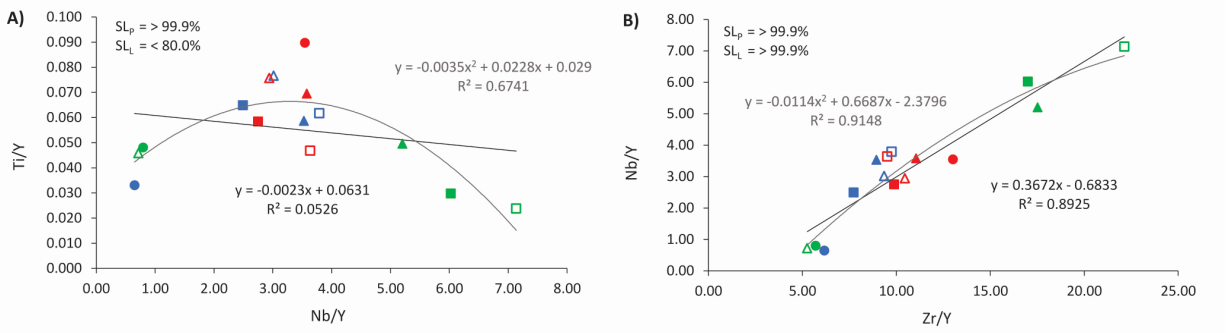

Figure 12. Harker diagrams of Ti/Y x Nb/Y and Nb/Y x Zr/Y for EG1, EG2 and EG3 wells rocks. Samples symbols are same as indicated in figure 11. SL_P = polynomial significance level; SL_L = linear significance level.

Figura 12. Diagramas de Harker de Ti/Y x Nb/Y and Nb/Y x Zr/Y para rochas dos poços EG1, EG2 e EG3. Símbolos das amostras são os mesmos que os indicados na figura 11. SL_P = nível de significância polinomial; SL_L = nível de significância linear.

Taking into consideration the complex geochemistry scenario presented above, it is evident the necessity to elaborate more robust geochemical models. Nevertheless, the generation of new geochemical data, especially isotopic, constitute a step to be carried out in the future.

Petrogenetic discussions and interpretations, mainly involving the behavior of trace elements and rare earths, will be presented separately for each well studied (Wells EG1, EG2 and EG3) below.

4.3.1. Well EG1

Despite some possible mobilization due to alteration, the major and trace element concentrations of the sidewall samples in Well EG1 – Section 1A are likely to represent magmatic compositions. For instance, the lower SiO_2 content of sample SPL 36 is largely coherent with its higher contents in MgO and compatible trace elements (Ni, Cr, Sc, Co, and V) and lower contents in incompatible elements (Rb, Sr, Nb, Y, Zr and Hf) when compared with more evolved (silica richer) samples SPL 37 and SPL 35 (Fig. 13). Samples SPL 35 and SPL 37 with similar SiO_2 contents (respectively, 54.23 and 55.02 wt.%) have also similar concentrations of immobile incompatible trace elements such as Nb (147 ppm), Zr (respectively, 415 ppm and 456 ppm) and Hf (8.6 ppm and 8.5 ppm).

In general, the magmatic section 1A represent a sequence of pyroclastic lithic ash tuffs with variable amounts of basalt scoria lithoclasts (more in mid-section; as represented by the least evolved sample SPL 37 and trachyte lithoclasts (towards the top and bottom of section; as represented by samples SPL 35 and SPL 36, respectively).

The pyroclastic tuffs SPL 35 and SPL 37 are intermediate rocks with SiO_2 values of 54.23 wt.% and 55.02 wt.%, respectively. Tuff SPL 33 is ultrabasic but the very low values in SiO_2 may also have resulted from some remobilization due to

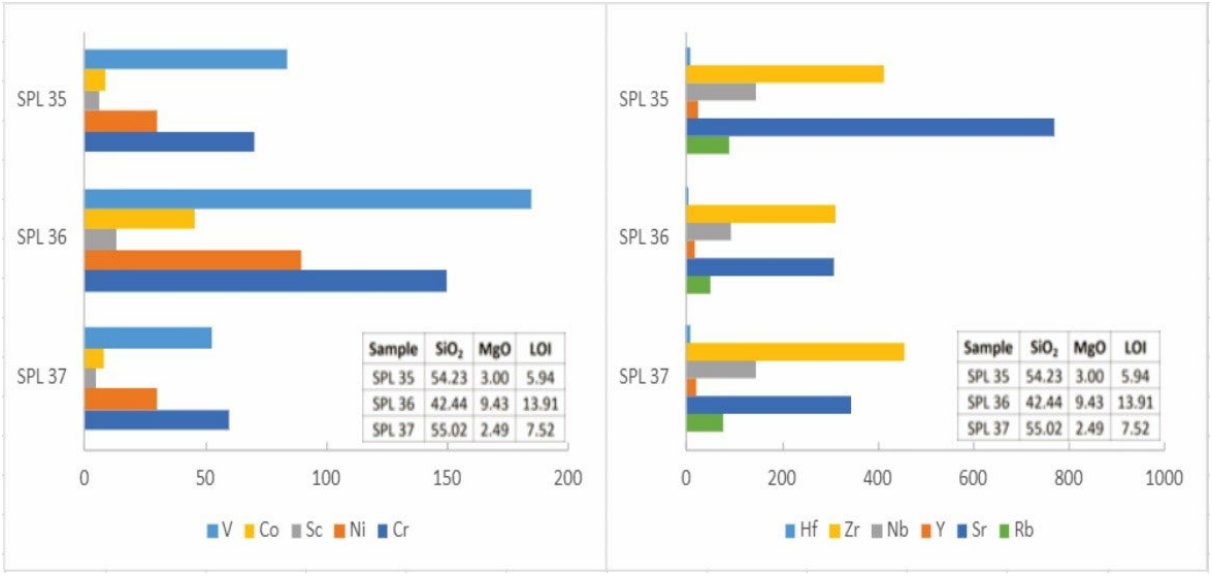

Figure 13. Concentrations (ppm) of selected compatible (Ni, Cr, Sc, Co, V) and incompatible (Hf, Zr, Nb, Y, Sr, Rb) elements of samples SPL 35, SPL 36 and SPL 37 in Well EG1. The SiO_2, MgO and LOI contents (in wt.%) of samples are indicated.

Figura 13. Concentrações (ppm) de elementos compatíveis (Ni, Cr, Sc, Co, V) e incompatíveis (Hf, Zr, Nb, Y, Sr, Rb) das amostras SPL 35, SPL 36 e SPL 37 no Poço EG1. As concentrações de SiO_2, MgO e LOI (em % peso) das amostras são indicadas.

alteration. The tuffs are alkaline (*e.g.* Nb/Y > 0.65; Pearce and Norry, 1979) miaskitic (Al/ (Na + K) >1.0, in mol. prop.) rocks and plot as potassic trachyte (SPL 35 and SPL 37) and basaltic trachyandesite (SPL 36) in the total alkalis *versus* silica (TAS) classification diagram (Fig. 10).

The samples display roughly subparallel patterns in chondrite-normalized multielement diagrams (Fig. 14). The more evolved samples SPL 35 and SPL 37 are more enriched in trace elements than the least evolved sample SPL 36 as expected if they were to be related by fractional crystallization in subvolcanic magma chambers. Troughs in Sr, P and Ti may be related to fractional crystallization of minor phases, such as apatite and oxides, included in phenocrysts. The existence of carbonate in sample SPL 49 can explain the enriched content of Rb, Sr and K (Figs. 14A, C and E). Fractional crystallization of amphibole involving the basaltic trachyandesite can explain the concave convex of its REE pattern (Figs. 14B, D and F). Nevertheless, the cross-cutting patterns of the three tuffs in REE chondrite-normalized diagrams (Figs. 14B and D) suggest that these rocks possibly have not evolved simply by fractional crystallization (Brod *et al.*, 2013) and more complex disequilibrium processes may have occurred in subvolcanic magma chambers (*ie.,* liquid immiscibility).

The patterns of the least evolved tuff (SPL 36) in normalized diagrams (Figs. 14A and B) are consistent with derivation from fertile, asthenospheric mantle sources based on its $La/Nb_{(N)}$ (< 1, *ie.*, lack of Nb trough) and $La/Yb_{(N)}$ (> 1) ratios. Geochemical

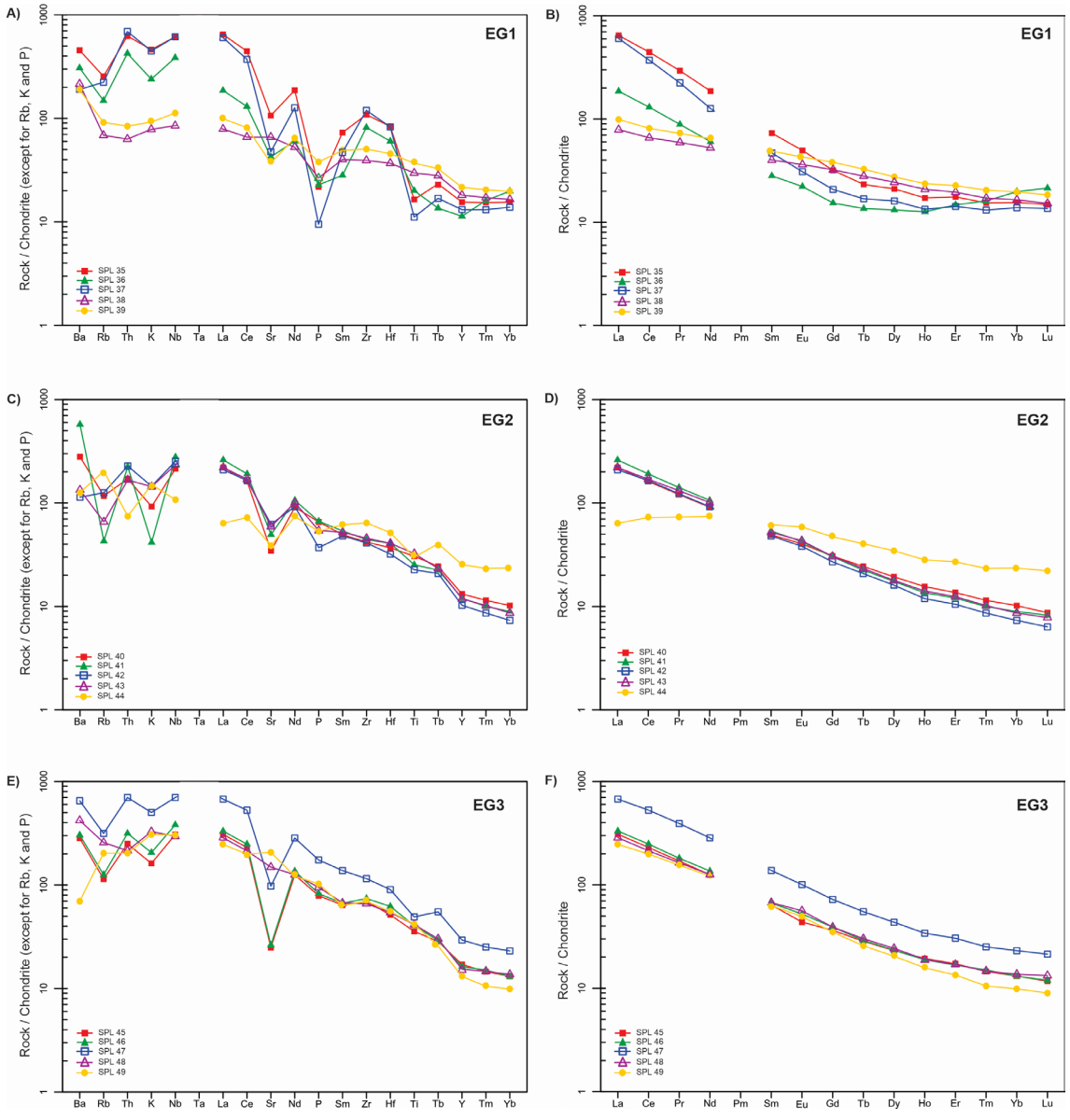

Figure 14. Normalized multielement diagram for samples of magmatic sections of wells EG1 (A), EG2 (C) and EG3 (E). Chondrite normalization factors are from McDonough and Sun (1995). Rb, K and P are from the primitive mantle of Sun (1980); REE chondrite-normalized diagram for samples of magmatic sections of wells EG1 (B), EG2 (D) and EG3 (F). Normalization factors from McDonough and Sun (1995).

Figura 14. Diagramas multielementares normalizados para amostras de seções magmáticas dos poços EG1 (A), EG2 (C) e EG3 (E). Os fatores de normalização dos condritos são de McDonough e Sun (1995). Rb, K e P são do manto primitivo do Sol (1980); Diagramas de ETRs normalizados a condrito para amostras de seções magmáticas dos poços EG1 (B), EG2 (D) e EG3 (F). Fatores de normalização de McDonough e Sun (1995).

modeling was applied to derive possible mantle source compositions of the magmas associated with magmatic section 1A of well EG1. Modeling was done using modal batch melting equations (*e.g.* Wood and Fraser, 1976) taking into consideration that alkaline basaltic magmas are derived from low degrees (<11%) of partial melting of lherzolitic mantle sources (*e.g.* Green, 2015). Modeling aimed to obtain the $La/Yb_{(N)}$ ratio of the least evolved sample SPL36 in the magmatic section at 10% partial melting of a lherzolitic source with residual Al-rich phase (garnet, spinel, or plagioclase). Results are shown in figure 15.

The $La/Yb_{(N)}$ ratio (~ 12) of typical OIB is just too high to generate the least evolved composition in the magmatic section, considering both the highest and lowest partition coefficients (Kd) values for Yb between garnet and alkaline basaltic magma. One solution for lherzolitic mantle with residual garnet required sources with $La/Yb_{(N)} < 1$ (0.59). However, this solution is unlikely to be applied since such trace element ratio is characteristic of plagioclase-bearing, depleted N-MORB mantle sources. A solution for lherzolitic mantle with residual plagioclase but $La/Yb_{(N)} > 1$ (4.35) is unlikely for similar reason. Possible solutions are either derivation from a more enriched ($La/Yb_{(N)}$ = 4.14) spinel lherzolite residual source or a less enriched ($La/Yb_{(N)}$ = 2.02) garnet lherzolite residual source. The former is consistent with the existence of a strongly attenuated lithosphere at the drifting stage of Campos Basin tectonic evolution.

In Section 1B, sample SPL 38 is more altered than sample SPL 39 as depicted by their LOI values (15.25 wt.% and 7.57 wt.%, respectively). Both samples are ultrabasic with relatively low MgO contents (3.29 wt.% and 4.56 wt.%, respectively). They are alkaline (*e.g.* Nb/Y > 0.65; Pearce and Norry, 1979) miaskitic (Al/(Na + K) > 1.0, in mol. prop.) rocks and the chemical classification will vary depending on the chosen diagram (Figs. 10 and 16), possibly because the recalculations required to plot samples in such diagrams are strongly affected by the LOI contents. As such, a classification as alkaline basalts seems appropriate based on immobile trace elements. In general, such classification seems more adequate than the modal classification, implying that samples in section 1B would rather be included in a mildly alkaline magmatic series rather than a strongly undersaturated one.

Samples display roughly parallel, weakly spiked patterns in chondrite-normalized multi-element diagrams (Fig. 14A) and REE chondrite-normalized diagrams (Fig. 14B), being consistent with fractional crystallization. The SiO_2 and MgO values of sample SPL 38 are likely to have been affected by alteration and may not represent magmatic values. The higher contents in immobile incompatible trace elements (*e.g.,* Zr, Hf, Nb, Y, Ti and REE) and lower contents in compatible trace elements (*e.g.,* Ni, Cr and Co) indicate that the mafic rock sample SPL 38 represents the more evolved magma composition. In addition, the similar $La/Nb_{(N)}$, $La/Yb_{(N)}$, $La/Sm_{(N)}$and $Gd/Lu_{(N)}$ ratios of samples SPL 38 and SPL 39 support a relationship by fractional crystallization.

The patterns of samples SPL 38 and SPL 39 in normalized diagrams (Fig. 14) are consistent with derivation from fertile, asthenospheric mantle sources based on its $La/Nb_{(N)}$ (<1, *ie.*, lack of Nb trough) and $La/Yb_{(N)}$ (> 1) ratios. The results of the modeling performed for magmatic section 1A can be used to derive possible mantle sources for the magmatic rocks in section 1B. Typical OIB compositions are too enriched in REE (*e.g.,* $La/Yb_{(N)}$ ~ 14) to give rise to least evolved alkaline basalt magmas with $La/Yb_{(N)}$ ~ 5 (Fig. 14B). The alkaline basalt magmas in section 1B could be related to either a more enriched ($La/Yb_{(N)}$ ~ 2) spinel lherzolite residual source or a less enriched ($La/Yb_{(N)}$ = 1) garnet lherzolite residual source. The former is consistent with the existence of a strongly

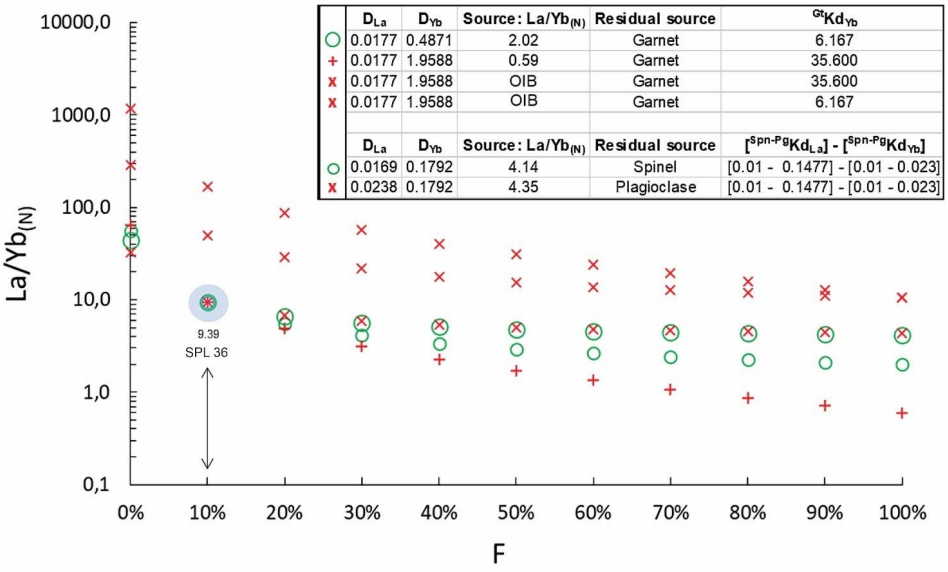

	D_{La}	D_{Yb}	Source: $La/Yb_{(N)}$	Residual source	$^{Gt}Kd_{Yb}$
○	0.0177	0.4871	2.02	Garnet	6.167
+	0.0177	1.9588	0.59	Garnet	35.600
x	0.0177	1.9588	OIB	Garnet	35.600
x	0.0177	1.9588	OIB	Garnet	6.167

	D_{La}	D_{Yb}	Source: $La/Yb_{(N)}$	Residual source	$[^{Spn-Pg}Kd_{La}] - [^{Spn-Pg}Kd_{Yb}]$
○	0.0169	0.1792	4.14	Spinel	[0.01 - 0.1477] - [0.01 - 0.023]
x	0.0238	0.1792	4.35	Plagioclase	[0.01 - 0.1477] - [0.01 - 0.023]

Figure 15. Results of modal batch partial melting modeling for the alkaline magmatism in section 1A of Well EG1. Modal compositions were 60% olivine, 20% orthopyroxene, 15% clinopyroxene and 5% of Al-rich phase (garnet (Gt), spinel (Spn) or plagioclase (Pg)). Partition coefficients (Kd) from table 4.1 in Rollinson (1993). OIB (ocean island basalt; $La/Yb_{(N)}$ ~ 12) composition from Sun and McDonough (1989). Normalization factors from McDonough and Sun (1995). $La/Yb_{(N)}$ of sample SPL 36 / EG1 (9.39, light blue circle) is indicated and can be derived from 10% partial melting. F is the amount of partial melting. $La/Yb_{(N)}$ of required sources are indicated.

Figura 15. Resultados da modelagem de fusão parcial modal para o magmatismo alcalino na seção 1A do Poço EG1. As composições modais foram 60% de olivina, 20% de ortopiroxênio, 15% de clinopiroxênio e 5% de fase rica em Al (granada (Gt), espinélio (Spn) ou plagioclásio (Pg)). Coeficientes de partição (Kd) da tabela 4.1 em Rollinson (1993). Composição OIB (basalto insular oceânico; La/Yb(N) ~ 12) de Sun e McDonough (1989). Fatores de normalização de McDonough e Sun (1995). La/Yb(N) da amostra SPL 36 / EG1 (9,39, círculo azul claro) é indicado e pode ser derivado de 10% de fusão parcial. F é a quantidade de fusão parcial. La/Yb(N) das fontes necessárias são indicadas.

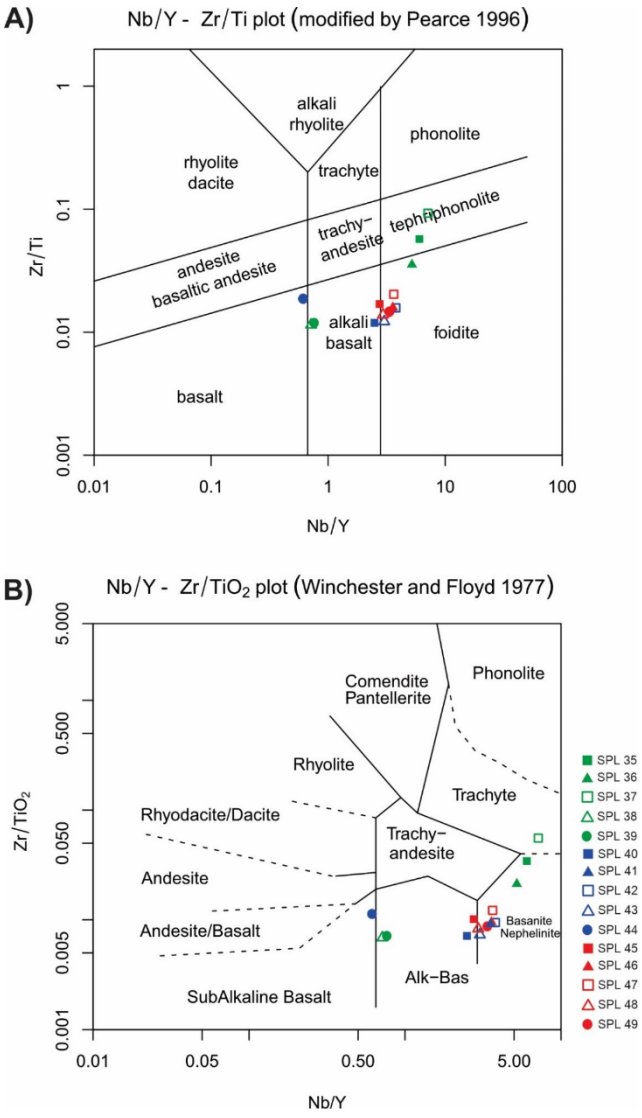

Figure 16. Sidewall core samples of wells EG1, EG2 and EG3 in Campos Basin plotted in classification diagrams based on immobile trace elements. A) Nb/Y versus Zr/Ti diagram (Pearce and Norry, 1979); B) Nb/Y versus Zr/TiO2 diagram (Winchester and Floyd, 1977). EG1 represented by green symbols, EG2 represented by blue symbols, EG3 represented by red symbols. Alk-Bas = alkaline basalt.

Figura 16. Amostras laterais dos poços EG1, EG2 e EG3 na Bacia de Campos plotadas em diagramas de classificação baseados em elementos traços imóveis. A) Diagrama Nb/Y versus Zr/Ti (Pearce e Norry, 1979); B) Diagrama Nb/Y versus Zr/TiO2 (Winchester e Floyd, 1977). EG1 representado por símbolos verdes, EG2 representado por símbolos azuis, EG3 representado por símbolos vermelhos. Alk-Bas = basalto alcalino.

attenuated lithosphere at the drifting stage of Campos Basin tectonic evolution, similar to the proposed model for section magmatic section 1A.

4.2.2. Well EG2

Lithogeochemical data obtained for the five sidewall core samples in magmatic section 2A of Well EG2 indicates that samples are altered as depicted by their high LOI values (> 20 wt.%) and their SiO_2 and MgO contents are unlikely to represent magmatic compositions. Alteration is likely to also have affected the concentrations of mobile trace elements, such as Ba, Sr and Rb. The concentrations of immobile trace elements (Y, Nb, Zr and Hf) are nearly invariable and the concentrations of Ni (100 - 550 ppm) and Cr (190 - 540 ppm) are relatively high and probably reflect the predominantly mafic compositions of the lithic lapilli tuffs in the magmatic section (Fig. 17). Comparable concentrations of Cr but different concentrations of Ni of samples SPL 41 and SPL 43 could be related to different amounts of clinopyroxene and olivine crystalloclasts in the tuffs, respectively.

Tuffs are mafic, alkaline rocks and plot in the alkaline basalt and foidite fields of the classification diagram based on immobile elements (Fig. 16A). The similar REE patterns of the four samples are also consistent with a nearly invariable composition of the tuffs (Fig. 14D).

Selected samples in magmatic section 2A display similar trace element patterns in the normalized multielement diagram (Fig. 14C). Spiked patterns for mobile trace elements (Ba, Rb, Th, K and Sr) are probably partially related to alteration. Smooth subparallel, almost superimposed patterns for immobile trace elements are consistent with a nearly invariable composition of the tuffs as aforementioned. In general, the immobile trace element compositions of the tuffs attest derivation from the same subvolcanic magma chambers unrelated to prolonged magma differentiation processes.

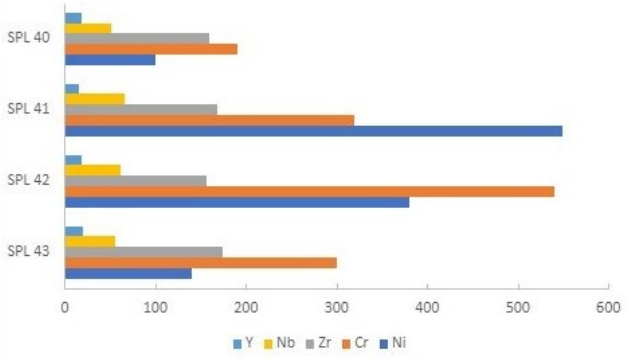

Figure 17. Concentrations (ppm) of selected compatible (Ni and Cr) and incompatible (Y, Nb and Zr) elements of samples SPL 40, SPL 41, SPL 42 and SPL 43 in Well EG2.

Figura 17. Concentrações (ppm) de elementos compatíveis (Ni e Cr) e incompatíveis (Y, Nb e Zr) selecionados das amostras SPL 40, SPL 41, SPL 42 e SPL 43 no Poço EG2.

The $La/Yb_{(N)}$ (>1; Fig. 14D) and $La/Nb_{(N)}$ (<1; Fig. 14C) ratios of the tuffs in magmatic section 2A indicate derivation from asthenospheric mantle sources. The $La/Yb_{(N)}$ ratios (~ 22 - 30) of the tuffs cannot be related to derivation from partial melting of typical OIB mantle sources ($La/Yb_{(N)}$ ~ 12) in the garnet stability zone (> 80 km) (Fig. 15). Derivation from asthenospheric lherzolites in the spinel stability zone (35 - 80 km) requires sources with $La/Yb_{(N)}$ ~ 9. Overall, the results of partial melting modeling indicate that the tuffs in magmatic section 2A of Well EG2 in Campos Basin are related to relatively shallow (35 - 80 km) depths of partial melting of asthenospheric sources.

Partial melting contributions from the enriched subcontinental lithospheric mantle and fertile, either typical OIB or plume-like (*e.g.* Trindade) are unlikely to be related to the studied lithic lapilli tuffs. These results may be related to the existence of a thin lithosphere in Campos Basin at the Santonian-Campanian allowing the uprising asthenosphere to melt at shallow depths.

According to the lithogeochemical data obtained for sidewall core SPL 44 (Section 2B), the lithic lapilli tuff is a mafic, alkaline rock and plot in the alkaline basalt field of the classification diagram based on immobile elements (Fig. 16).

The $La/Nb_{(N)}$ (< 1; Fig.14C) and $La/Yb_{(N)}$ (>1; Fig. 14D) ratios of the tuffs in magmatic section 2B indicate derivation from asthenospheric mantle sources. The $La/Yb_{(N)}$ ratio (2.7) of the tuffs cannot be related to derivation from partial melting of typical OIB mantle sources ($La/Yb_{(N)}$ ~ 12) in the garnet stability zone (> 80 km) (Fig. 15). Derivation from asthenospheric lherzolites in the spinel stability zone (35 - 80 km) or plagioclase stability zone (< 35 km) require sources with $La/Yb_{(N)}$ ~ 1 - 1.2. Overall, the results of partial melting modeling indicate that the tuffs in magmatic section 2B of Well EG2 in Campos Basin are possibly related to relatively shallow depths of partial melting of asthenospheric sources with the contribution of a more enriched mantle source. Partial melting contributions from the enriched subcontinental lithospheric mantle and fertile, either typical OIB or plume-like (*e.g.*, Trindade) are unlikely to be related to the studied lithic lapilli tuffs. These results may be related to the existence of a thin lithosphere in Campos Basin at the Santonian-Campanian allowing the uprising asthenosphere to melt at shallow depths.

4.2.3. Well EG3

Lithogeochemical data obtained for four sidewall core samples in magmatic sections 3A and 3B of Well 3 indicates that the samples are altered as depicted by their high LOI values (11 - 18 wt.%) and are classified mostly as foidites in the classification diagram based on immobile trace elements (Fig. 16A). Despite their similar classification, ash tuff SPL 47 represents the most evolved composition sampled in the magmatic section (Fig. 18).

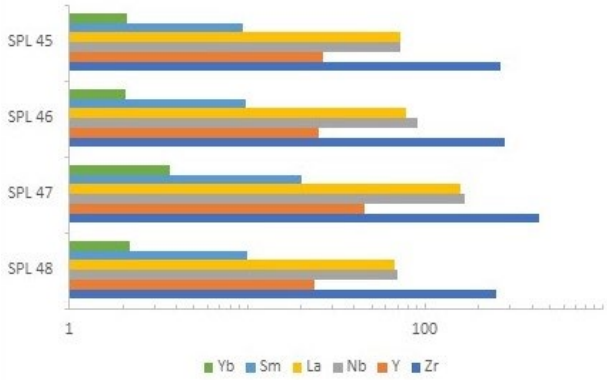

Figure 18. Concentrations (ppm) of selected incompatible, immobile elements of samples SPL 45, SPL 46, SPL 47, and SPL 48 of magmatic section 3A in Well EG3.

Figura 18: Concentrações (ppm) de elementos incompatíveis e imóveis selecionados das amostras SPL 45, SPL 446, SPL 47 e SPL 48 da seção magmática 3A no Poço EG3.

The more evolved composition of ash tuff SPL 47 is consistent with its higher values of the REE (Fig. 14F) and the whole set of trace elements (Fig. 14E). The little variation in REE ratios indicates that the evolved ash tuff and less evolved basaltic scoria are related by fractional crystallization in subvolcanic magma chambers.

The $La/Yb_{(N)}$ (>1; Fig. 14F) and La/Nb(N) (≤1; Fig. 14E) ratios of these samples indicate derivation from asthenospheric mantle sources. The $La/Yb_{(N)}$ ratios (~ 21 - 29) of the samples cannot be related to derivation from partial melting of typical OIB mantle sources ($La/Yb_{(N)}$ ~ 12) in the garnet stability zone (> 80 km) (Fig. 15). Derivation from asthenospheric lherzolites in the spinel stability zone (35 - 80 km) requires sources with $La/Yb_{(N)}$ ~ 9. Overall, the results of partial melting modeling indicate that the samples in magmatic sections 3A and 3B of Well EG3 in Campos Basin are related to relatively shallow (35 - 80 km) depths of partial melting of asthenospheric sources. Partial melting contributions from the enriched subcontinental lithospheric mantle and fertile, either typical OIB or plumelike (*e.g.*, Trindade) are unlikely to be related to the studied volcanic rocks. These results may be related to the existence of a thin lithosphere in Campos Basin at the Santonian-Campanian allowing the uprising asthenosphere to melt at shallow depths.

Lithogeochemical data obtained for section 3C indicates that sample SPL 49 plots in the foidite field in the classification diagram based on immobile trace elements (Fig. 15A). The high LOI content of the sample attests to its alteration as also depicted by the petrography.

Sample SPL 49 has $La/Nb_{(N)}$ = 0.8, $La/Yb_{(N)}$ = 25.0, $La/Sm_{(N)}$ = 3.9 and $Gd/Lu_{(N)}$ = 3.9 attesting derivation from asthenospheric mantle sources. Geochemical modeling indicates that partial melting took place in the spinel stability field (35 - 80 km) and involved a source with $La/Yb_{(N)}$ ~ 9.0. This composition is unlikely to be related to contributions from either the subcontinental lithospheric mantle or OIB-like deep mantle components. Overall, the magmatic section 3C of Well EG3 seems related to partial melting of the ascending asthenosphere beneath an attenuated lithosphere in the Santonian-Campanian time. Conclusions related to magmatic section 3C are the same presented previously for magmatic sections 3A and 3B of Well EG3 in Campos Basin.

5. Discussion

5.1. Well EG1

The following inferences can be made based on the petrographic and lithogeochemical data obtained for Well EG1:

Section 1A is a 66 m thick section formed by lithic ash and lapilli tuffs with variable amounts of basaltic scoria and trachyte lithoclasts. Tuffs are likely to result from bimodal (alkaline basalt-trachyte), mildly alkaline, subaerial explosive volcanism. These pyroclastic rocks represent deposits formed by explosive volcanism from stratovolcanoes in marine environments but high enough to emerge above sea level. Besides that, a little reworking of volcanoclasts took place in a deposition site close to the emission center.

The pyroclastic tuffs are chemically similar to the bentonite thin layers of the 3-Fingers Mark (Marco 3 Dedos) and 3B Mark (Marco 3B). However, section 1A comprises thick (66 m-size) layers of pyroclastic tuff that are neither epiclastic nor related to ash falls. In addition, emission centers seem to be proximal as opposed to those at the continent proposed for the bentonites and ash tuffs elsewhere in Campos.

Explosive eruptions that gave rise to the pyroclastic tuffs in section 1A could have been less energetic (possibly Strombolian or Vulcanian) than the Plinian eruptive styles associated with the bentonites in Campos. Low-magnitude earthquakes and debris flow may be expected to be associated with such explosive eruptions.

Section 1B is a 22 m thick section formed by alkaline diabases that are likely to result from bimodal (alkaline basalt trachyte), mildly alkaline magmatism.

The intrusive or effusive type of magmatism is difficult to ascertain based on well data, petrography and lithogeochemistry.

However, the viscosity of alkaline basaltic lava flows is low enough to allow spreading over relatively large areas from the emission center. Such flows would easily reach the subaqueous depositional environment of the sedimentary rocks of the Campos Group, but no textures indicative of subaqueous volcanism have been observed in the studied samples.

Samples of diabases also display little amounts of glass and are medium-to-coarse-grained, as opposed to glass-rich, very fine-grained textures found in typical basaltic flows. Altogether, the alkaline samples in magmatic section 1B are likely to represent either a chemically differentiated, single or multiple magmatic intrusions. If the magmatic section represents multiple intrusions, the alkaline diabases would be magmas associated with fractional crystallization in shallow, subvolcanic magma chambers.

Partial melting processes in both sections involved asthenospheric mantle sources and took place in depths either related to stable garnet (> 80 km) or stable spinel (35 - 80 km). It is unlikely that the precursor alkaline magmas related to the samples can be associated exclusively with either typical OIB or MORB asthenospheric mantle sources. Derivation from spinel-bearing lherzolitic asthenospheric sources could be related to the existence of an attenuated lithosphere during the drifting stage of Campos Basin.

The following conclusions can be made for the drift-related magmatism recorded in Well EG1 based on the aforementioned interpretations of the petrological data of magmatic sections 1A and 1B:

1. It represents a mildly alkaline, miaskitic series whose either spinel- or garnet-lherzolite mantle sources are less enriched in trace incompatible elements than typical OIB.
2. The pyroclastic tuffs interbedded with the siliciclastic sedimentary rocks of the Campos Group cannot be associated with the typical bentonites and ash falls of the 3-Fingers and 3B-Marks in Campos Basin. They represent the products of subaerial, Strombolian to Vulcanian explosions of high-standing stratovolcanoes that emerged above sea level. The pyroclastics underwent restricted transport from the emission center.
3. The alkaline diabases occur possibly as sills and intrude the shallow marine shales and marls of the Ubatuba Formation. Major temperature increments that might have affected potential petroleum systems due to this intrusion would be relevant for marls and shales at 50 m or less above and below the intrusion.

5.2. Well EG2

The following conclusions can be made based on the petrographic and lithogeochemical data obtained for Well EG2:

Both sections 2A (483.5 m thick) and 2B (54 m thick) are lithic lapilli tuffs. These rocks are probably related to low-intensity, subaqueous explosive eruptions (phreatomagmatism) from monogenetic, small scoria cones. Monogenetic, small scoria cones are the most common volcanic edifices associated with basaltic scoria and usually occur in clusters. Brittle structures such as normal and listric faults can be found at the base of scoria cones since they are commonly subjected to subsidence.

Tuffs have nearly invariable trace element compositions predominantly mafic, alkaline rocks. As such, no or limited differentiation process in either deep-seated or subvolcanic magma chambers and pumbling systems is expected and heat conduction to upper levels should be negligible. Hydrothermal processes may have occurred due to interactions of erupted lavas and shallow marine waters.

In both sections, partial melting processes involved asthenospheric mantle sources in the spinel or plagioclase stability zone (< 35 - 80 km) and are unlikely to have involved only the subcontinental lithospheric mantle (SCLM) and either typical OIB or plume-like mantle components.

5.3. Well EG3

The following conclusions can be made based on the petrographic and lithogeochemical data obtained for magmatic sections 3A, 3B and 3C of Well EG:

They comprise various occurrences of magmatic rocks interlayered with the sedimentary rocks of the Ubatuba Formation. Magmatic occurrences vary from 1 m to 168 m in thickness.

Basaltic scoria, ash tuff, lapilli tuff and alkaline basalt were sampled along the magmatic sections. They represent extrusive and pyroclastic deposits predominantly less welded and mafic but also more welded, more evolved ash tuffs. These rocks are related to subaerial explosive eruptions from stratovolcanoes that may grow above sea level in marine environments.

Variations in trace element compositions indicate that less and more evolved rocks can be related by fractional crystallization in subvolcanic magma chambers and related pumbling systems. As such, heat conduction to upper levels may be expected. Hydrothermal processes may have been restricted due to the predominantly mafic composition of the lavas.

Partial melting processes involved asthenospheric mantle sources in the spinel or plagioclase stability zone (< 35 - 80 km) and are unlikely to have involved only the subcontinental lithospheric mantle and either typical OIB or plume-like mantle components.

6. Conclusion

6.1. The drift-related magmatism in Cabo Frio High area

The interpretation of well-log, petrographic and lithogeochemical data obtained for magmatic sections located above the salt sequence in wells EG1, EG2 and EG3 were previously presented in this paper. Even before any geochronological data can be obtained, we can infer that the magmatic rocks are taken as representative of the drift-related, Santonian-Campanian magmatism in Campos Basin (Winter *et al.*, 2007). The magmatic sections comprised volcanic rocks, diabases, and phaneritic, massive igneous rocks according to well profiles. Rock classifications were fined based on petrographic descriptions under macro and microscales (Tab. 1).

The following conclusions can be made so far about the drift-related magmatism in the study area based on the interpretation of the petrological data:

1. It is mostly explosive and volcanic. The only intrusion (alkaline diabase) was found in magmatic section 1B of well EG1.
2. Volcanic edifices in marine environments are: a) composite stratovolcanoes high enough to stand above sea level giving rise to subaerial explosive and effusive eruptions; b) small, monogenetic scoria

cones either parasitic in stratovolcanoes or below sea water.

3. It is alkaline and includes mostly mafic rocks (alkaline basalt, basanite/nephelinite and foidite) with subordinate felsic rocks (tephriphonolite, trachyte) (Fig. 16).
4. Heat conduction due to magmatic differentiation in subvolcanic magma chambers and related pumbling systems is minimum. Heat due to sill intrusion in EG1 has not been conducted beyond about 50 m away from the contacts.
5. Hydrothermal processes may have been relevant in areas with scoria cones due to interactions with seawater and not because of the composition of the magmas, which are represented by mafic, dry alkaline basalts, basanites and foidites.

Table 1. Classification of rocks in magmatic sections studied.

Tabela 1. Classificação das rochas nas seções magmáticas estudadas.

Well	Section	Well profile	Petrography
EG1	1A	Dark grey, massive volcanic rock	Lithic, ash and lapilli tuffs
EG1	1B	Grey diabase	Alkaline diabase
EG2	2A	Volcanic rock.	Lithic lapilli tuffs.
EG2	2B	Grey diabase	Lithic lapilli tuffs
EG3	3A	Volcanic rock.	- Highly vesiculated, less massive basaltic scoria - Less vesiculated, more massive basaltic scoria - Highly vesiculated, less massive basaltic scoria - Welded ash tuff
EG3	3B	Volcanic Rock	- Welded Lapilli tuff - Alkaline Basalt
EG3	3C	Diabase.	Welded lapilli tuff

A main discussion on the drift-related (or post-breakup) magmatism in sedimentary basins offshore Brazil (Campos included) refers to thermal regimes associated with partial melting processes in the underlain mantle. It is an obvious issue to be addressed since heat is fundamental for hydrocarbon generation in these basins, also affecting the quality of potential reservoirs due to associated hydrothermalism. The usual petrological approach to assess partial melting regimes in the mantle is to use the composition of the least evolved rocks. The trace element ratios and isotope compositions of these rocks are the closest representation of the composition of their mantle sources. Differentiation indexes, such as MgO and SiO_2, can be used to select the least evolved compositions in a set of samples. However, these major elements can change due to alteration, and this seems to be the case for most of the samples in the studied area, whose LOI contents vary from 6 wt.% to 26 wt.%. On the other hand, immobile trace elements such as Zr, Y, Nb and Ti are likely to represent magmatic compositions even in altered samples. These elements are also incompatible during crystal-liquid equilibria processes, such as partial melting, meaning that their concentrations will be the lowest in the least evolved samples. Selected trace elements and LOI concentrations for sidewall core samples in the wells of Campos Basin are listed in table 2.

Sample SPL 35 in well EG1 has the lowest LOI concentration among all sidewall core samples in the studied area. It has high concentrations in Zr, Y, Nb, Hf, La and Yb, and low concentrations in Ni and Cr as would be expected from more evolved magmatic compositions. Sample SPL 47 in well EG3 also has high and low concentrations in incompatible and compatible trace elements, respectively, despite its higher LOI content. On the other hand, sample SPL 38 in well EG1 with high LOI has low and high concentrations in incompatible and compatible trace elements which is consistent with a less evolved magmatic composition. The same applies to sample SPL 41 in well EG2 with much higher LOI contents. Thus, the sample that is more likely to represent trace element ratios compositions of its respective mantle source would be SPL 38, based on its relatively low LOI concentrations, as well as low concentrations in incompatible elements and high concentrations in compatible elements (Tab. 2). This sample was taken from a 22 m thick intrusion of alkaline diabase (Tab. 1) and its composition may have been less affected by the complex differentiation processes that usually take place in subvolcanic magma chambers. On the other hand, sample SPL 41 in well EG2 is a lithic lapilli tuff (Tab. 1) with high LOI contents (Tab. 2) that has been associated with subaqueous explosive volcanism (Tab. 2). However, this sample presents no evidence for changes in REE concentrations due to interactions with seawater such as Ce anomalies, for instance, and its composition may truly reflect those of its respective mantle source. Thus, it is note worthing that the $La/Yb_{(N)}$ ratios of samples SPL 38 and SPL 41 have a 6-fold difference (Tab. 2). Despite differences, the $La/Yb_{(N)}$ and $La/Nb_{(N)}$ ratios of samples SPL 38 and SPL 41, respectively above and below the unity (Tab. 2) cannot be explained by derivation from asthenospheric, shallow, depleted, MORB-like mantle sources ($La/Yb_{(N)} < 1$), but are typical of OIB-like, asthenospheric sources ($La/Yb_{(N)} = 11.6$; $La/Nb_{(N)} = 0.78$, (McDonough and Sun, 1989). There is much discussion in the literature about the mantle components involved in OIB-like sources regarding origins in the fertile (incompatible element-rich) deep mantle

Table 2. Selected lithogeochemical data of sidewall core samples with different alteration degrees in the studied magmatic sections. LOI in wt.%. Trace elements in ppm. Normalization factors (N) used for trace element ratios are from McDonough and Sun (1995).

Tabela 2. Dados litogeoquímicos selecionados de amostras laterais com diferentes graus de alteração nas seções magmáticas estudadas. LOI em % peso. Elementos traço em ppm. Os fatores de normalização (N) usados para razões de elementos traço são de McDonough e Sun (1995).

Wells	Samples	LOI	Ni	Cr	Zr	Y	Nb	Hf	La	Yb	$La/Nb_{(N)}$	$La/Nb_{(N)}$
EG1	SPL 35	5.94	30	70	415	24.4	147	8.6	153	2.5	1.05	41.6
EG3	SPL 47	11.21	30	20	440	46.2	168	9.3	160	3.72	0.96	29.2
EG1	SPL 38	15.25	120	130	150	28.5	20	3.8	18.7	2.66	0.93	4.8
EG2	SPL 41	23.27	550	320	169	18.9	67	4.2	61.8	1.44	0.94	29.2

(such as mantle plumes) or shallow but equally fertile mantle depths. In addition, the involvement of the subcontinental lithospheric mantle source (typically $La/Nb_{(N)} > 1$) would easily produce $La/Nb_{(N)}$ ratios below unit, even considering binary mixing processes with fertile, deep OIB-like mantle components.

The cross-cutting REE patterns of samples SPL 38 and SPL 41 (Fig. 19) cannot be explained by different amounts of partial melting from the same mantle source. Therefore, either one or both of them do not represent their mantle sources compositions for being changed during differentiation or they are related to derivation from different mantle sources. The latter being true, the higher normalized REE ratios of sample SPL 41 implies partial melting of a more enriched mantle source than the one melted to give rise to sample SPL 38.

Alkaline basalts and basanites primary melts derived from 1 - 11% partial melting of lherzolites according to experimental petrology studies. Lherzolites are peridotites with high amounts of olivine (generally, > 50%), more clinopyroxene than orthopyroxene and about 5-10% of an Al-rich phase that can be plagioclase (< 35 km), spinel (35 - 80 km) or garnet (> 80 km). The low degree of partial melting (< 11%) to generate alkaline basalts implies that it is likely that the Al-rich phase will not melt completely and will remain as a residual phase in the melted lherzolite. In other words, melting is likely to be modal, *ie.* the proportions between phases in the melted lherzolite will be very similar to that in the original lherzolite. In addition, the segregation of melts from the source will not be instantaneous, meaning that partial melting will occur in equilibrium as opposed to fractional.

Modeling of modal batch (equilibrium) melting was elaborated in order to test for possible mantle sources and depths of melting capable of explaining the $La/Yb_{(N)}$ ratios of samples SPL 38 and SPL 41 of wells EG1 and EG2 in Campos Basin and results are shown in figure 20.

Results indicate that melting of typical OIB and Trindade plume at depths below 80 km (garnet stability zone) cannot explain neither the low nor the high $La/Yb_{(N)}$ ratios of the sidewall core samples. Melting of OIB-like mantle sources can explain the high $La/Yb_{(N)}$ ratio of sample SPL 41 but much less enriched asthenospheric sources ($La/Yb_{(N)}$ = 2.2) would be required to explain the composition of sample SPL 38. Finally, although a typical, N-MORB mantle source could generate the low $La/Yb_{(N)}$ ratio of sample SPL 38 it can hardly explain the $La/Nb_{(N)}$ ratio (< 1) of the studied samples.

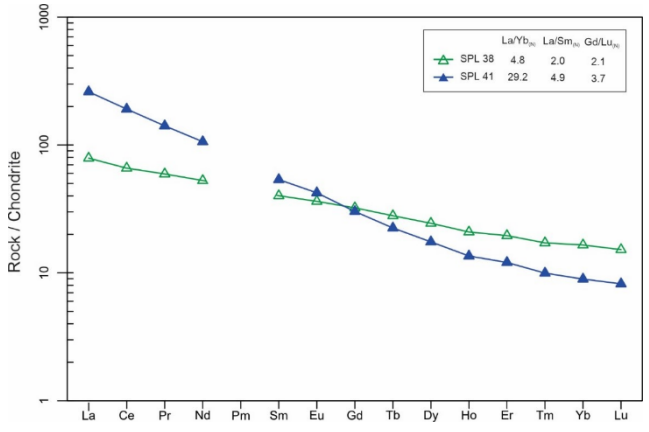

Figure 19. REE chondrite-normalized diagram for samples SPL 38 and SPL 41 in Campos Basin. Normalization factors from McDonough and Sun (1995). Wells and selected trace element ratios are indicated.

Figura 19. Diagrama ETR normalizado a condrito para amostras SPL 38 e SPL 41 na Bacia de Campos. Fatores de normalização de McDonough e Sun (1995). Poços e razões de elementos traços selecionados são indicados.

The results of the geochemical modeling and the lithogeochemical data allow inferring that the studied drift magmatism in Campos is related to shallow (35 - 80 km) mantle depths of partial melting. The process seems not to have involved the subcontinental lithospheric mantle, implying the presence of an attenuated lithosphere that allowed the uprising of the underlying asthenosphere. This asthenosphere was neither exclusively depleted (N-MORB type) nor only very enriched (OIB-like of Trindade plume-like). As such, mantle temperatures can be taken as "normal" (~ 1325 - 1430°C; Green, 2015) as opposed to higher temperatures proposed for mantle plume-related magmatism (~ 300°C higher than surrounding mantle; White and McKenzie, 1989; Campbell, 2007; Spice *et al.*, 2016).

Once lithogeochemical compositions of the studied samples in wells EG1, EG2 and EG3 cannot be attributed to derivation from partial melting of a single mantle source, mixing processes were then taken into consideration.

Incompatible, immobile trace element ratios of major mantle sources and samples SPL 38, SPL 41 are listed in table 3. References for N-MORB, OIB, Trindade Plume and SCLM are listed. The trace element ratios of samples SPL 38 and SPL 41 were taken as representative of the less and more enriched mantle sources below wells EG1 and EG2, respectively. They have trace element ratios that may reach a 6-fold difference (e.g. $La/Yb_{(N)}$), likely to represent the involvement of compositionally different mantle sources in their petrogenesis (Fig. 21A).

The analytical mixing model presented below was constrained using the equations presented in Faure (1994). Element ratios of four immobile, incompatible trace elements (La, Y, Zr and Nb) were used in the modelling. The aim of the model is to discriminate two mantle source end members whose mixing can explain the less and more enriched trace element ratios of samples SPL 38 (well EG1) and SPL 41 (well EG2).

Mixing between fertile mantle sources, such as OIB and the Trindade mantle-plume and between them and enriched mantle sources (SCLM1 to SCLM4) are unsuitable to produce mixing curves capable of fitting the compositions of either sample SPL 41 or SPL 38 or even both, as can be depicted by the compositions of these sources in table 3. Particularly, the La/Y ratio (0.7) of the less enriched sample SPL 38 requires the involvement of a depleted mantle source, such as N-MORB, in the mixing process. On the other hand, OIB and Trindade mantle plume compositions are just not enriched enough to produce the enriched trace element ratios of sample SPL 41 when mixed with N-MORB. Therefore, the likely end members in the mixing process would be N-MORB and the SCLM

The SCLM is probably the most heterogeneous of mantle sources since it is attached to the continental crust throughout geological time. As such, it is difficult to constrain its chemical compositions. However, ultrapotassic-potassic, ultramafic, ultrabasic-basic rocks, such as lamproites and lamprophyres, are probably the best representative of the SCLM compositions, according to many authors (e.g. Rock, 1991).

The binary mixing model presented below was done considering 4 possible compositions to represent the SCLM underneath the studied area (Tab. 3). SCLM1 is an average lamproite composition (Rock, 1991) whereas the other are average compositions of lamprophyres in São Paulo coastline (SCLM2), Rio de Janeiro coastline (SCLM3) and in Atalaia Peninsula (SCLM4). The Atalaia Peninsula area is taken as the onshore

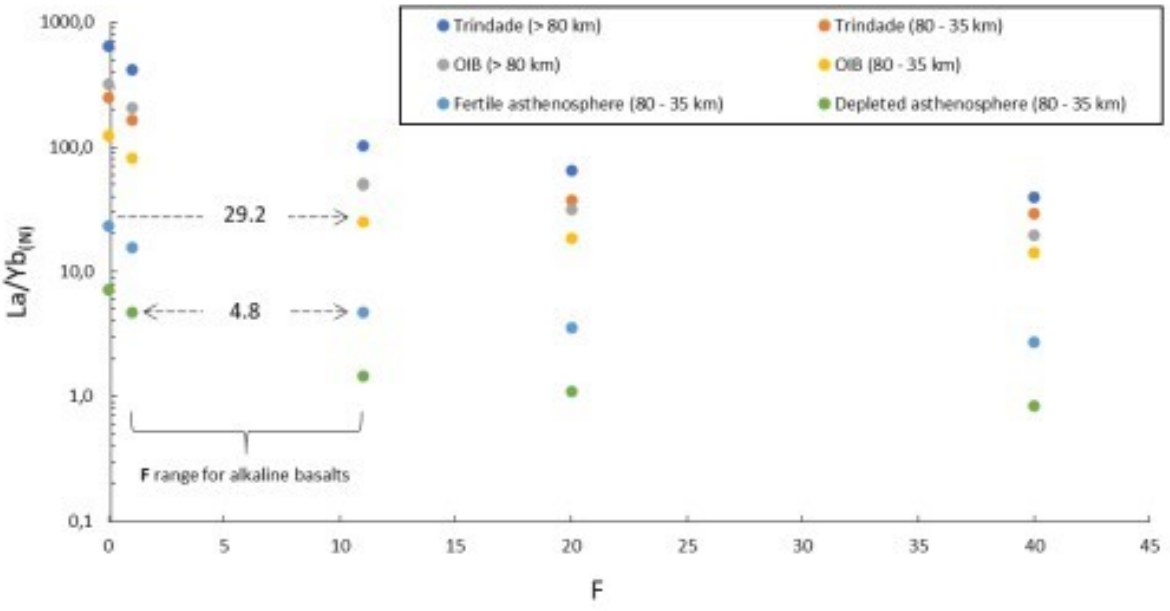

	Depth of melting (km)	Depth of melting (km)	Depth of melting	Depth of melting	Depth of melting	Depth of melting
	> 80	80-35	> 80	80-35	80-35	80-35
	Residual phase	**Residual phase**	**Residual phase**	**Residual phase**	**Residual phase**	**Residual phase**
	Garnet	Spinel	Garnet	Spinel	Spinel	Spinel
	$La/Yb_{(N)}$ - Trindade	**$La/Yb_{(N)}$ - Trindade**	**$La/Yb_{(N)}$ - OIB**	**$La/Yb_{(N)}$ - OIB**	**$La/Yb_{(N)}$**	**$La/Yb_{(N)}$**
	23.5	23.5	11.6	11.6	2.2	0.7
F (%)	**$La/Yb_{(N)}$ - melt**	**$La/Yb_{(N)}$ - melt**	**$La/Yb_{(N)}$ - melt**	**$La/Yb_{(N)}$ - melt**	**$La/Yb_{(N)}$ - melt**	**$La/Yb_{(N)}$ - melt**
0	644,3	248,3	317,5	122,4	23,4	7,2
1	**418,9**	**164,2**	**206,4**	**80,9**	**15,5**	**4,8**
11	**101,3**	**50,5**	**49,9**	**24,9**	**4,8**	**1,5**
20	64,5	37,7	31,8	18,6	3,6	1,1
40	39,5	29,0	19,5	14,3	2,7	0,8

Figure 20. Results of geochemical modeling of modal batch partial melting process related to the drift magmatism in Campos Basin. See Wood and Fraser (1976) and references therein for equations and fundamentals. Trindade data from Siebel *et al.* (2000). OIB data from McDonough and Sun (1989). F is the degree of partial melting (in %). Normalization factors (N) from McDonough and Sun (1995). The La/Yb(N) ratios of samples SPL 38 (4.9) and SPL 41 (29.2) are indicated by dashed arrows.

Figura 20. Resultados da modelagem geoquímica do processo de fusão parcial relacionado ao magmatismo drifte na Bacia de Campos. Veja Wood e Fraser (1976) e as referências nele contidas para equações e fundamentos. Dados de Trindade de Siebel *et al.* (2000). Dados OIB de McDonough e Sun (1995). F é o grau de fusão parcial (em %). Fatores de normalização (N) de McDonough e Sun (1995). As razões La/Yb(N) das amostras SPL 38 (4.9) e SPL 41 (29.2) são indicadas por setas tracejadas.

representation of the Cabo Frio Structural High between Campos and Santos basins, close to which studied wells are located offshore. Results of the mixing model are presented in figure 21A.

The SCLM1 composition is too enriched and unsuitable as an end-member component with mixing processes involving N-MORB. On the other hand, SCLM2 (São Paulo lamprophyres) and SCLM3 (Rio lamprophyres) do not have compositions enriched enough to generate the trace element ratios of SPL 41. The best fitting of a mixing curve was obtained for N-MORB and SCLM4. It is noteworthing that SCLM4 is the average composition of lamprophyres that crop out in the continental area that represents the Cabo Frio Structural High.

The results of the modelling indicate the geodynamic processes that took place in the Cabo Frio High area during the Santonian-Campanian, involved mixing between a depleted, relatively shallow asthenospheric source (N-MORB) and the local subcontinental lithospheric mantle represented by the average composition of the lamprophyres at the Cabo Frio Structural High (SCLM4). Different amounts of mixing are required to explain the less and more enriched compositions of samples SPL 38 and SPL 41, as such: about 87% N-MORB and 13% SCLM4 (sample SPL 38) and about 20% N-MORB and 80% SCLM4 (sample SPL 41).

Another binary mixing model was done to try to reproduce the cross-cutting relationships of chondrite-normalized REE patterns and the $La/Yb_{(N)}$ ratios of samples SPL 41 and SPL 38 and results are shown in figure 21B. Modelling was done using average values of the REE for the same samples used to calculate the SCLM4 composition, i.e. the lamprophyres on the Cabo Frio Structural High in the continental area adjoining Santos Basin). The model reproduced with good approximation the cross-cutting patterns and exactly the same $La/Yb_{(N)}$ ratios of the two samples (Fig. 21B). The amount of end members in the mixing process is very close to that obtained in the previous modelling (Fig. 21A) with a predominant and subordinate role for N-MORB in the petrogenesis of the magmatic rocks in wells EG2 and EG1, respectively.

Table 3. Incompatible, immobile trace element ratios (La/Y and Zr/Nb) of major mantle sources and samples SPL 41 and SPL 38. SCLM1 to SCLM4 are taken as potential representative compositions of the subcontinental lithospheric mantle near studied area.

Tabela 3. Razões de elementos traços incompatíveis e imóveis (La/Y e Zr/Nb) das principais fontes do manto e amostras SPL 41 e SPL 38. SCLM1 a SCLM4 são consideradas potenciais composições representativas do manto litosférico subcontinental próximo à região estudada.

Reference	**Source**	**La/Y**	**Zr/Nb**
Sun & McDonough, 1989	NMORB	0.1	31.8
Sun & McDonough, 1989	OIB	1.3	5.8
Basanite dyke 10764 (Siebel *et al.*, 2000)	Trindade	2.5	2.3
Lamproite (Rock, 1991)	SCLM1	15.5	8.6
Average lamprophyres SP (Valente, 1997)	SCLM2	2.1	4.3
Average lamprophyres RJ (Valente, 1997)	SCLM3	2.5	1.8
Average lamprophyres Cabo Frio High (Valente, 1997)	SCLM4	4.1	3.4
Composition	**Sample**	**La/Y**	**Zr/Nb**
Less enriched	SPL 38	0.7	7.5
More enriched	SPL 41	3.3	2.5

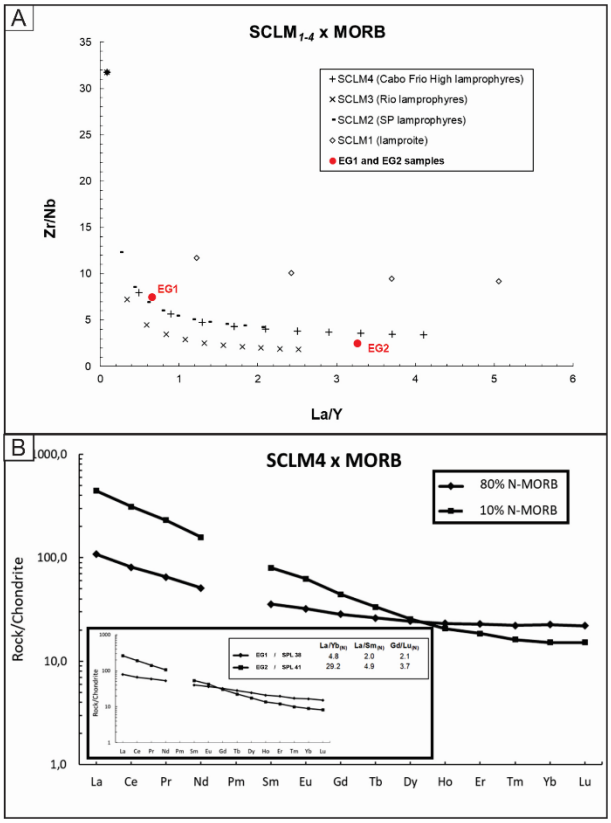

Figure 21. A) results of binary mixing analytical modelling between potential mantle sources. Mixing curves (diamond; cross; dash; x) at 10% intervals between N-MORB and four different subcontinental lithospheric mantle compositions (SCLM1 to SCLM4). Samples SPL 38 (less enriched) and SPL 41 (more enriched) from wells EG2 and EG3, respectively, are also plotted in the diagram. Source and sample compositions are shown in table 3; B) results of binary mixing analytical modelling between N-MORB and SCLM4.

Figura 21. A) resultados da modelagem analítica de mistura binária entre potenciais fontes mantélicas. Curvas de mistura (diamante; cruz; traço; x) em intervalos de 10% entre N-MORB e quatro diferentes composições do manto litosférico subcontinental (SCLM1 a SCLM4). As amostras SPL 38 (menos enriquecidas) e SPL 41 (mais enriquecidas) dos poços EG2 e EG3, respectivamente, também estão representadas no diagrama. As composições de fonte e amostra são mostradas na tabela 3; B) resultados da modelagem analítica de mistura binária entre N-MORB e SCLM4.

In conclusion, the analytical binary mixing models presented in this section suggest that N-MORB and the subcontinental lithospheric mantle (SCLM) interacted during the geodynamic processes occurring in the Santonian-Campanian within the Cabo Frio High area. However, the potential contribution of other enriched sources can still be considered, and further geochemical and isotopic studies are required to determine the extent of their involvement. The interaction of different sources in the generation of these magmas is supposed to have occurred in a thinned continental lithosphere, allowing the depleted asthenosphere to rise up to the stability zone (35 - 80 km), as supported by Rigoti (2015) geophysical-geological modeling for the Santos Basin. Partial melting of the depleted asthenosphere would result from adiabatic decompression, while smaller melt fractions could be generated in the enriched SCLM due to thermal conduction from the convecting asthenosphere below. Melting temperatures in the asthenosphere are believed to be slightly higher than those of the normal mantle (~ 1270 °C), whereas lower temperatures would be required to melt the volatile-rich, enriched SCLM. Partial melting of more enriched and fusible portions or veins within the SCLM could account for the higher proportion of this end member in the mixing models. Ascending melts could accumulate and install plumbing systems within the thin (~ 10-15 km) brittle upper mantle, providing a feeding pathway for the stratovolcanoes above.

Acknowledgements

We acknowledge the support and funding from Equinor Brazil and the support of ANP (Brazil's National Oil, Natural Gas and Biofuels Agency) through the R&D levy regulation. Master's student Tatiele Marques Jatobá de Barros acknowledges CAPES scholarship, a research funding agency in Brazil.

Data privacy

The precise location and coordinates of the samples studied in this scientific paper are not given. In addition, the identifier codes of these samples have also been changed. These actions were necessary due to a confidentiality clause in the research project signed between Equinor Brazil and the Federal Rural University of Rio de Janeiro.

Complementary Material

Whole-rock major and trace element compositions of EG1, EG2 and EG3.

References

Almeida, F. F. M., 1983. Relações tectônicas das rochas alcalinas Mesozóicas da região meridional da Plataforma Sul-Americana. *Revista Brasileira de Geociências*, **13**(3): 139-158.

Almeida, F. F. M., Carneiro, C. R., Mizusaki, A. M., 1996. Correlação do magmatismo das bacias da margem continental Brasileira com a das áreas emersas adjacentes. *Revista Brasileira de Geociências*, **26**(3): 125-138.

Almeida, J., Heilbron, M., Guedes, E., Neubauer, F., Manfred, B., Klausen, M. B., Valeriano, C. M., Bruno, H., Giro, J. P., McMaster, M., Tetzner, W., 2021. Pre-to-syn-rift tholeiitic magmatism in a transtensive hyperextended continental margin: Onshore and offshore magmatism in the Campos Basin, SE Brazil. *Journal of South American Earth Sciences*, **108**: 103218. https://doi.org/10.1016/j.jsames.2021.103218.

Alves, D. B., 2006. Sedimentação vulcanoclástica do Cretáceo Superior da Bacia de Campos, Sudeste do Brasil. *Boletim de Geociências da Petrobras*, **14**: 149-154.

Brod, J. A., Junqueira-Brod, T. C., Gaspar, J. C., Petrinovic, I. A., Valente. S. C., Corval, A., 2013. Decoupling of paired elements, crossover REE patterns, and mirrored spider diagrams: Fingerprinting liquid immiscibility in the Tapira alkaline-carbonatite complex, SE Brazil. *Journal of South American Earth Sciences*, **41**: 41-56. https://doi.org/10.1016/j.jsames.2012.04.013.

Caddah, L. F. G., Alves, D. B., Hanashiro, M., Mizusaki, A. M. P., 1994. Caracterização e origem do marco "3-Dedos" (Santoniano) da Bacia de Campos. *Boletim de Geociências da Petrobras*, **8**: 315-334.

Campbell, I. H., 2007. Testing the plume theory. *Chemical Geology*, **241**(3-4): 153-176. https://doi.org/10.1016/j.chemgeo.2007.01.024.

Castro, R. D., Picolini, J. P., 2014. Principais aspectos da geologia regional da Bacia de Campos. *In*: Kowsmann, R.O. (Ed.), *Geologia e Geomorfologia. Rio de Janeiro: Elsevier. Habitats*, **1**: 1-12. https://doi.org/10.1016/B978-85-352-6937-6.50008-2.

Chang, H. K., Assine, M. L., Correa, F. S., Tinen, J. S., Vidal, A. C., Koike, L., 2008. Sistemas petrolíferos e modelos de acumulação de hidrocarbonetos na Bacia de Santos. *Revista Brasileira de Geociências*, **38**: 29-46. https://doi.org/10.25249/0375-7536.2008382S2946.

Dani, A. P. O., Remus, M. V. D., Dani, N., Lima, E. F., 2017. Magmatismo basáltico do Andar Alagoas (Bacia de Campos). *Geologia USP, Série Científica*, **17**: 269-287. https://doi.org/10.11606/issn.2316-9095.v17-373.

De Luca, P., Carballo, J., Filgueiras, A., Pimentel, G., Esteban, M., Tritlla, J., Villacorta, R., 2015. What is the Role of Volcanic Rocks in the Brazilian Pre-salt? *In*: European Association of Geoscientists and Engineers, *77th EAGE Conference and Exhibition 2015*, 1-5. https://doi.org/10.3997/2214-4609.201412890.

Faure, G., 1986. Principles of isotope geology. *John Wiley & Sons*, New York, 590.

Fodor, R. V., McKee, E. H., Asmus, H. E., 1983. K-Ar Ages and the opening of the South Atlantic Ocean: basaltic rock from the Brazilian margin. *Marine Geology*, **54**(1-2): M1-M8. https://doi.org/10.1016/0025-3227(83)90002-6.

Fodor, R. V., Vetter, S. K., 1984. Rift-zone magmatism: Petrology of basaltic rocks transitional from CFB to MORB, southeastern Brazil margin. *Contributions to Mineralogy and Petrology*, **88**: 307-321. https://doi.org/10.1007/BF00376755.

Franke, Dieter, 2013. Rifting, lithosphere breakup and volcanism: Comparison of magma-poor and volcanic rifted margins. *Marine and Petroleum Geology*, **43**: 63-87. https://doi.org/10.1016/j.marpetgeo.2012.11.003.

Green, D. H., 2015. Experimental petrology of peridotites, including effects of water and carbon on melting in the Earth's upper mantle. *Physics and Chemistry of Minerals*, **42**: 95-122. https://doi.org/10.1007/s00269-014-0729-2.

Gordon, A. C., Mohriak, W. U., Santon, N., Santos A. C., 2023. Magmatic cycles in Santos Basin (S.E. Brazil): Tectonic control in the temporal-spatial distribution and geophysical signature. *Journal of South American Earth Sciences,* **121**, 104111. https://doi.org/10.1016/j.jsames.2022.104111.

Heilbron, M., Mohriak, W. U., Valeriano, C. M., Milani, E. J., Almeida, J., Tupinambá, M., 2000. From collision to extension: the roots of the southeastern continental margin of Brazil. *In*: Mohriak, W.; Tankard, U. (Eds), *Atlantic Rifts and Continental Margins American Geophysical Union*, Geophysical Monograph Series, **115**: 1-32. https://doi.org/10.1029/GM115p0001.

Irvine, T. N., Baragar, W. R. A., 1971. A guide to the chemical classification of the common volcanic rocks. *Canadian Journal of Earth Sciences*, **8**: 523–548. https://doi.org/10.1139/e71-055.

Le Bas, M. J., Le Maitre, R. W., Streckeisen, A., Zanettin, B., 1986. A chemical classification of volcanic rocks based on the Total Alkali-Silica Diagram. *Journal of Petrology*, **27**(3): 745-750. https://doi.org/10.1093/petrology/27.3.745.

Lobo, J. T., 2007. *Petrogênese de rochas basálticas do Eocretáceo das Bacias de Campos e Pelotas e implicações na geodinâmica de rifteamento do Gondwana Ocidental*. Tese de Doutorado, FGEL-UERJ, 250.

Macedo, J. M., 1989. Evolução tectônica da Bacia de Santos e áreas continentais adjacentes. *Boletim de Geociências da Petrobrás*, **3**: 159-173.

McDonough, W. F., Sun, S., 1995. The composition of the Earth. *Chemical Geology*, **120**: 223-253. https://doi.org/10.1016/0009-2541(94)00140-4.

Miyashiro, A., 1978. Nature of alkalic volcanic rock series. *Contributions to Mineralogy and Petrology*, **66**(1), 91-104. https://doi.org/10.1007/BF00376089.

Mizusaki, A. M. P., Petrini, R., Bellieni, G., Comin-Chiaramonti, P., Dias, J., De Min, A., Picirillo, E. M., 1992. Basalt magmatism along the passive continental margin of SE Brazil (Campos basin). *Contributions to Mineralogy and Petrology*, **111**: 143-160. https://doi.org/10.1007/BF00348948.

Mizusaki, A. M. P., Mohriak, W. U., 1992. Sequências vulcanosedimentares na região da plataforma continental de Cabo Frio, RJ. *In*: *Resumos Expandidos,* 37, Congresso Brasileiro de Geologia, São Paulo, SP, **2**: 468-469.

Mohriak, W. U., De Barros, A. Z. N., 1990. Novas evidências de tectonismo cenozóico na região Sudeste do Brasil: O Graben de Barra de São João, na plataforma de Cabo Frio, RJ. *Revista Brasileira de Geociências*, **20**(1–4): 187-196.

Mohriak, W. U., Macedo, J. M., Castelani, R. T., Rangel, H. D., Barros, A. Z. N., Latgé, M. A. L., Ricci, J. A, Mizusaki, A. M. P., Szatmari, P., Demercian, L. S., Rizzo, J. G., Ayres, J. R., 1995. Salt Tectonics and Structural Styles in the Deep – Water Province of the Cabo Frio Region, Rio de Janeiro, Brazil. *In*: Jackson D.G., Roberts, D.G., Snelson S. (Eds.), *Salt Tectonics: A Global Perspective. AAPG Memoir*, **65**: 273-304.

Mohriak, W. U., 2003. Bacias Sedimentares da Margem Continental Brasileira. *In*: C. S. L. A. Bizzi, R. M. Vidotti e J. H. Gonçalves (Eds.), *Geologia, Tectônica e Recursos Minerais do Brasil*. Brasília, DF, Brasil, CPRM, **1**: 87-165.

Mohriak, W. U., Gordon, A., Mello, M. R., 2021. Origin and Petroleum System of the Cabo Frio High Between Santos and Campos Basins: Reviewed Integration of Structural and Paleogeographic Reconstruction with the Oil and Gas Systems. *In*: Mello, M. R., Yilmaz, P. O., Katz, B. J. (Eds), *The Supergiant Lower Cretaceous Pre-Salt Petroleum Systems of the Santos Basin, Brazil: AAPG Memoir 124. AAPG Special Volumes*, 273-324. https://doi.org/10.1306/13722323MSB.11.1853.

Moreira, J. L. P., Esteves, C. A., Rodrigues, J. J. G., Vasconcelos, C. S., 2005. Magmatismo, sedimentação e estratigrafia da porção norte da Bacia de Santos. *Boletim de Geociências da Petrobrás*, **14**(1), 161-170.

Moreira, J. L. P., Madeira, C.V., Gil, J. A., Machado, M. A. P., 2007. Bacia de Santos. *Boletim de Geociências da Petrobras*, **15**(2), 531-549.

Oreiro, S. G., Guerra, M. C. M., 2005. Expressão sísmica de eventos magmáticos e não-magmáticos na Bacia de Santos. *Anais do 11 Simpósio de Vulcanismo e Ambientes Associados*, Cabo Frio, 195-200.

Oreiro, S. G., 2006. Magmatismo e sedimentação em uma área na Plataforma Continental de Cabo Frio, Rio de Janeiro, Brasil, no intervalo Cretáceo Superior–Terciário. *Boletim de Geociências da Petrobras*, **14**: 95-112.

Oreiro, S. G.; Cupertino, J. A., Szatmari, P., Thomaz Filho, A., 2008. Influence of pre-salt alignments in post-Aptian magmatism in the Cabo Frio High and its surroundings, Santos and Campos basins, SE Brazil: An example of non-plume-related magmatism. *Journal of South American Earth Sciences*, **25**: 116-131. https://doi.org/10.1016/j.jsames.2007.08.006.

Pearce, J. A., Norry, M. J., 1979. Petrogenetic implications of Ti, Zr, Y and Nb variations in intrusive rocks. *Contributions to Mineralogy and Petrology*, **69**: 33-47. https://doi.org/10.1007/BF00375192.

Pearce, J. A., 1996. A user's guide to basalt discrimination diagrams. *In*: D. A. Wyman (Ed.), Trace element geochemistry of volcanic rocks: applications for massive sulphide exploration. *Geological Association of Canada*, **12**: 79-113.

Pedro, A. J., 2005. *Utilização da sismoestratigrafia no estudo da atuação do alto de Cabo Frio sobre a sedimentação na porção sul da Bacia de Campos.* Dissertação de mestrado, Lagemar, UFF, Niterói, RJ, Brasil, 97.

Rancan, C. C., Oliveira, L. C., De Carmo, I. O., Marins, G. M., Pessoa, V. C. O., De Andrade, H., Penatti, A. P. R., Borges, T. A.; Da Silva, R. C. B., Carlotto, M. A., Bassetto, M., Zanatta, A. S., 2018. Rochas ígneas do Bloco de Libra, Bacia de Santos. *Anais do 49° Congresso Brasileiro de Geologia,* 2012.

Rangel, 2006. Manifestações magmáticas na parte sul da Bacia de Campos (Área de Cabo Frio) e na Bacia de Jequitinhonha. *Boletim de Geociências da Petrobras*, **14**(1): 155-160.

Riccomini, C., Fernandez, V. V., Gomes, C., 2005. Tectonic controls of the Mesozoic and Cenozoic alkaline magmatism in central-southern Brazilian Platform. *In*: Comin-Chiaramonti, P., Gomes, P. B. (Eds.), Mesozoic to Cenozoic alkaline magmatism in the Brazilian Platform. *EDUSP-FAPESP*, 31-56.

Rigoti, C. A., 2015. *Evolução tectônica da Bacia de Santos com ênfase na geometria crustal: Interpretação integrada de dados de sísmica de reflexão e refração, gravimetria e magnetometria*. Dissertação de mestrado, FGEL-UERJ, Rio de Janeiro, RJ, Brasil, 134.

Rock, N. M. S., 1991. Lamprophyres. *Glasgow: Blackie and Son Ltd*, 285.

Rollinson, H. R., 1993. *Using geochemical data: evaluation, presentation, interpretation*. Routledge, New York, USA, 384.

Schmitt, R. S., Trouw, R. A. J., Van Schmus, W. R., Pimentel, M. M., 2004. Late amalgamation in the central part of West Gondwana: new geochronological data and the characterization of a Cambrian orogeny in the Ribeira Belt (SE Brazil). Precambrian Research, 133, 29-61. https://doi.org/10.1016/j.precamres.2004.03.010.

Schmitt, R. S., Van Schmus, W. R., Trouw, R. A. J., Passchier, C. W., 2008. Cambrian orogeny in the Ribeira Belt (SE Brazil) and correlations within West Gondwana: Ties that bind underwater. *Geological Society, Special Publications*, **294**: 279-296. https://doi.org/10.1144/SP294.15.

Schober, P., Boer, C., Schwarte L. A., 2018. Correlation Coefficients: Appropriate Use and Interpretation. *Anesth Analg*., **126**(5): 1763-1768. https://doi.org/10.1213/ANE.0000000000002864.

Siebel, W., Becchio, R., Volker, F., Hansen, M. A. F., Viramonte, J., Trumbull, R. B., Haase, G., Zimmer, M., 2000. Trindade and Martín Vaz Islands, South Atlantic: isotopic (Sr, Nd, Pb) and trace element constraints on plume related magmatism. *Journal of South American Earth Sciences*, **13**(1-2): 79-103. https://doi.org/10.1016/S0895-9811(00)00015-8.

Spice, H. E., Fitton, J. G., Kirstein, L. A., 2016. Temperature fluctuationof the Iceland mantle plume through time. *Geochemistry, Geophysics, Geosystems*, **17**(2): 243-254. https://doi.org/10.1002/2015GC006059.

Sun, S. S., 1980. Lead isotopic study of young volcanic rocks from mid-ocean ridges, ocean islands and island arcs. *Philosophical Transactions of The Royal Society. Series A, Mathematical, Physical and Engineering Sciences*, **297**: 409-445. https://doi.org/10.1098/rsta.1980.0224.

Sun, S. S., McDonough, W. F., 1989. Chemical and isotopic systematics of oceanic basalts; implications for mantle composition and processes. *In*: A. D. Saunders, M. J. Norry (Eds.), *Magmatism in the ocean basins*. London: Geological Society of London, **42**: 313-345. https://doi.org/10.1144/GSL.SP.1989.042.01.19.

Thomaz-Filho, A., Rodrigues A. L., 1999. O alinhamento de rochas alcalinas Poços de Caldas-Cabo Frio (RJ) e sua Continuidade na Cadeia Vitória-Trindade. *Revista Brasileira de Geociências*, **29**(2): 189-194.

Thomaz-Filho, A., Cesero, P., Mizusaki, A. M., Leão, J. G., 2006. Hot spot volcanic tracks and their implications for South American plate motion, Campos basin (Rio de Janeiro state), Brazil. *Journal of South American Earth Sciences*, **18**: 383-389. https://doi.org/10.1016/j.jsames.2004.11.006.

Thomaz-Filho, A., Mizusaki, A. M. P, Antonioli, L., 2008. Magmatismo nas bacias sedimentares brasileiras e sua influência na geologia do petróleo*. Revista Brasileira de Geociências*, **38**(2): 128-137.

Thompson, R. N., Gibson, S. A., Mitchell, J. G., Dickin, A. P., Leonardos, O. H., Brod, J. A., Greenwood, J. C., 1998. Migrating Cretaceous – Eocene Magmatism in the Serra do Mar Alkaline provinces, SE Brazil: melts from the deflected Trindade Mantle Plume? *Journal of Petrology*, **39**(8): 493-526. https://doi.org/10.1093/petroj/39.8.1493.

Tupinambá, M., Heilbron, M., Duarte, B. P., Nogueira, J. R., Valladares, C., Almeida, J., Eirado Silva, L. G., Medeiros, S. R., Almeida, C. G., Miranda, A., Ragatky, C. D., Mendes, J., Ludka, I., 2007. Geologia da Faixa Ribeira Setentrional: Estado da arte e conexões com a Faixa Araçuaí. *Genomos*, **15**(1): 67-79. https://doi.org/10.18285/geonomos.v15i1.108.

Valente, S. C., 1997. *Geochemical and isotopic constraints on the petrogenesis of the Cretaceous dykes of Rio de Janeiro, Brazil*. Belfast, PhD. Thesis, The Queen's University of Belfast, 366.

White, R., McKenzie, D., 1989. Magmatism at rift zones: the generation of volcanic continental margins and flood basalts. *Journal of Geophysical Research: Solid Earth*, **94**(B6): 7685-7729. https://doi.org/10.1029/JB094iB06p07685.

Winchester, J. A., Floyd, P. A., 1977. Geochemical discrimination of different magma series and their differentiation products using immobile elements. *Chemical Geology*, **20**: 325-343. https://doi.org/10.1016/0009-2541(77)90057-2.

Winter, R. W., Jahnert, R. J., França, A. B., 2007. Bacia de Campos. *Boletim de Geociências da Petrobras*, **15**: 511-529.

Wood, B., J., Fraser, D. C., 1976. *Elementary thermodynamics for geologists*. Oxford University Press, Oxford, England, 303.

Zalan, P. V., Oliveira, J. A. B., 2005. Origem e Evolução Estrutural dos Riftes cenozóicos do Sudeste do Brasil. *Boletim de Geociências da Petrobras*, **13**(2): 269–300.

Complementary material: Whole-rock major and trace element compositions of EG1, EG2 and EG3.

Material complementar: Composição dos elementos de traço e maiores de rocha total das amostras EG1, EG2 e EG3.

Well	EG1	EG1	EG1	EG1	EG1	EG2	EG2	EG2	EG2	EG2	EG3	EG3	EG3	EG3	EG3
Sample	SPL 35	SPL 36	SPL 37	SPL 38	SPL 39	SPL 40	SPL 41	SPL 42	SPL 43	SPL 44	SPL 45	SPL 46	SPL 47	SPL 48	SPL 49
SiO_2 (wt%)	54.23	42.44	55.02	37.12	44.31	32.41	25.57	30.85	30.11	39.12	33.83	37.54	45.88	38.71	33.88
$Al2O_3$	17.02	12.88	17.7	16.18	14.64	11.35	7.62	7.37	9.64	13.92	12.73	13.98	20.05	12.06	12.24
Fe_2O_3(T)	6.34	7.81	4.04	10.73	12.15	8.01	7.45	7.45	8.32	16.25	11.06	13.38	6.59	9.77	6.28
MnO	0.079	0.113	0.054	0.162	0.183	0.152	0.176	0.106	0.086	0.529	0.186	0.196	0.016	0.223	0.16
MgO	3	9.43	2.49	3.29	4.56	4.01	7.81	6.46	5.34	2.57	4.73	4.26	0.7	4.74	5.41
CaO	1.8	5.28	1.08	11.18	7.53	15.28	21.58	15.18	16.13	4.73	9.16	4.35	2.7	9.49	13.77
Na_2O	4.11	3.21	5.14	3.6	5.36	4.29	1.67	1.45	1.93	4.18	3.83	1.35	1.45	2.56	2.57
K_2O	6.3	2.97	5.98	0.97	1.24	1.06	0.45	1.52	1.58	1.87	1.89	2.42	6.49	4.06	3.66
TiO_2	1.209	1.471	0.816	2.176	2.709	2.24	1.85	1.658	2.376	2.191	2.609	2.969	3.606	3.043	3.067
P_2O_5	0.23	0.24	0.1	0.28	0.4	0.69	0.7	0.39	0.57	0.56	0.83	0.87	1.84	1	1.08
LOI	5.94	13.91	7.52	15.25	7.57	19.95	23.27	25.95	22.86	14.02	17.52	17.06	11.21	14.68	17.84
Sc (ppm)	6	13	5	27	31	21	19	19	17	22	11	12	8	28	12
Be	3	3	3	1	1	1	1	1	1	2	2	3	3	2	2
V	84	185	53	192	241	223	177	121	268	187	183	223	186	258	233
Cr	70	150	60	130	40	190	320	540	300	< 20	< 20	< 20	20	240	180
Co	9	46	8	55	33	31	101	37	36	33	24	34	18	28	42
Ni	30	90	30	120	40	100	550	380	140	40	30	40	30	110	90
Cu	10	30	10	50	70	50	50	30	40	< 10	20	20	10	30	30
Zn	80	80	50	40	90	70	70	70	80	60	50	100	< 30	60	60
Ga	22	16	20	17	18	15	13	11	14	16	17	20	30	18	18
Ge	1.2	1.2	1.1	1	1.3	1	0.8	0.9	1.1	1.3	0.6	0.7	1.3	1.4	1
As	< 5	5	< 5	7	< 5	< 5	< 5	< 5	< 5	< 5	< 5	< 5	10	< 5	< 5
Rb	89	52	78	24	32	41	15	44	23	71	40	44	110	90	71
Sr	772	308	345	478	269	250	358	451	428	280	180	190	707	1078	1501
Y	24.4	17.8	20.6	28.5	33.8	20.7	18.9	16.1	18.6	39.7	26.8	25.6	46.2	24.1	20.5
Zr	415	312	456	150	193	160	169	157	174	245	265	283	440	252	267
Nb	147	92.6	147	20.4	27	51.6	66.7	61	56.1	25.8	73.7	91.6	168	70.9	72.7
Mo	3	< 2	3	< 2	2	< 2	< 2	< 2	< 2	< 2	5	5	9	8	17
Ag	1.6	1.2	1.8	0.7	0.8	0.7	0.7	0.6	0.7	0.8	0.8	1	1.9	1	1